# Study of Diffusion in Confined Nanospace

Sneha

Technische Universiteit Delft

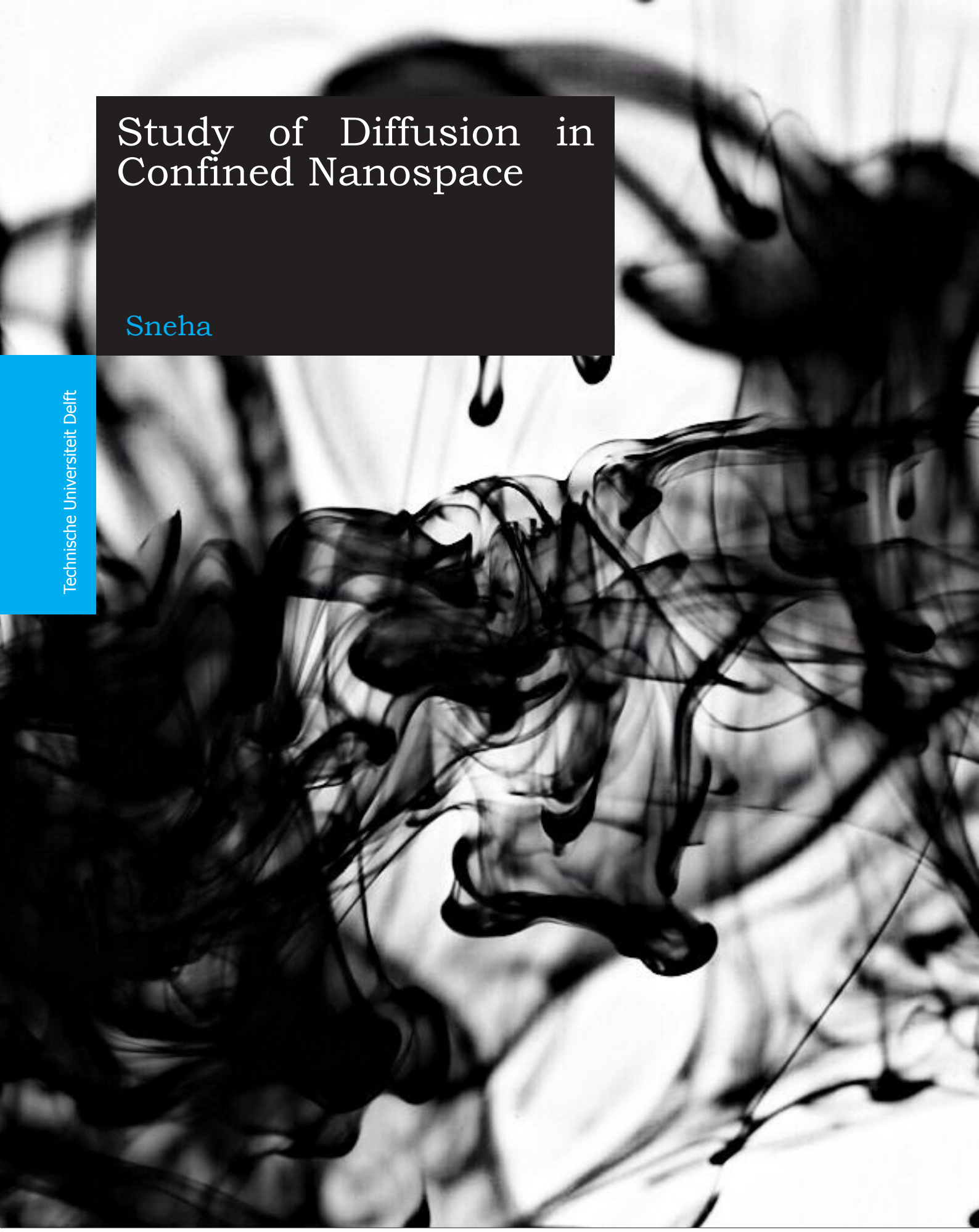

TU Delft Delft University of Technology

Challenge the future

# Study of Diffusion in Confined Nanospace

by

**Sneha**

in partial fulfillment of the requirements for the degree of

**Master of Science**
in Chemical Engineering

at the Delft University of Technology,
to be defended publicly on Wednesday August 16, 2017 at 3:00 PM.

| | | |
|---|---|---|
| Supervisors: | Prof. Dr. E. J. R. Sudholter | |
| | Dr. Volkert van Steijn | |
| Thesis committee: | Prof. Dr. E. J. R. Sudholter, | TU Delft |
| | Dr. Volkert van Steijn, | TU Delft |
| | Dr. David Vermaas | TU Delft |

*This thesis is confidential and cannot be made public until December 31, 2017.*



TU Delft Delft University of Technology

# Abstract

The cellular environment is characterized by confinement and macro-molecular crowding: both concepts that have been studied separately. To understand kinetics of enzymatic reactions, there is a need to understand how the diffusional encounters of enzyme and substrate proceed in an environment that is confined and crowded simultaneously. The project carried out in this thesis is the first step towards achieving the ultimate goal of studying biochemical reactions in native cellular environment - Understanding diffusion in confinement. Despite multiple investigations of diffusion of analytes in confinement, there exists a research gap. There is inconsistency in the interpretation of the results and in the dependence of diffusion properties of analytes of different sizes in channels of different dimensions. Hence, to bridge the research gap, the main goal of this thesis project was to find the diffusion coefficient of 100 nm polystyrene beads in microchannel (200 $\mu$m wide and 4.5 $\mu$m high) and nanochannel (5 or 10 $\mu$m wide and 300 nm high). The Brownian motion of particles was observed using Confocal Laser Scanning Microscope. A preliminary study first confirmed the reliability and optimization of the particle tracking method of finding diffusion coefficient. Diffusion coefficient of the particles determined experimentally in microchannel (bulk system) was in agreement with the theoretical estimate and statistically significant. Experiments in the nanochannel revealed a reduction in the particle diffusion coefficient of about ~52% compared to bulk, due to interactions with the confining depth (300 nm) of nanochannel. An interesting behaviour was also exhibited by particles diffusing close to the side wall along the width of nanochannels, which was not confining (5 or 10 $\mu$m). The diffusion coefficient in such a case reduced by around ~90% relative to bulk. The reduction in both cases can be mainly attributed to hydrodynamic interactions. The experimental investigations of diffusion coefficient carried out in this study were in agreement with long standing theoretical predictions. However, the research gap could not be fully expelled.

*Sneha*
*Delft, August 2017*

# Acknowledgement

This thesis project has been a long journey, for which I would like to express my gratitude towards many. First and foremost, I would like to thank Prof. Dr. E.J.R. Sudholter and Dr. Volkert van Steijn for being my supervisors. This project would not have been possible without their guidance, motivation and support throughout. I feel privileged to be guided by them, to be their student and to learn from them. There was always something to takeaway from their wealth of knowledge in every meeting that I had. I also extend my gratitude to Dr. David Vermaas who accepted my invitation to be a member of my thesis defense committee.

I express my gratitude towards Eugene for helping me out with the cleanroom procedure. I would also like to thank Hamid for being my cleanroom mentor. Without his help, I wouldn't have been able to start my project. I cannot thank enough Sumit for his unstinting support and help. He has been there to clear every little doubt I had from the beginning till the end of this project. I want to thank Rajiv and Naveen for being there and motivating me. I would like to thank Lukasz for always being available for discussions. I would also like to extend my gratitude to all the other OMI members for creating such a happy place to work in. The group outings were always a stress buster.

I am thankful to Serhii, from the ASM group, for finding time in his schedule to help me with the microscope. I extend my gratitude to Wim, Shaurya, Kartik and Jishnu, from the PPE group, for helping me find my way in the lab. They have been very kind to always answer my questions. I also would like to thank the other master students from the PPE group. It has been a nice experience sharing the workplace with them. I would like to express my gratitude to Somnath from Denmark for sharing his knowledge with me. His inputs greatly helped me to understand concepts related to the thesis topic. I want to thank all my friends at the university for being there and listening to me when I needed them. Their presence and support has kept me going.

Last but not the least, I want to thank people who were thousands of miles away, but their support made a difference - my family and Rachit. I cannot imagine completing this roller coaster journey without their love, support and faith in me.

*Sneha*
*Delft, August 2017*

# Contents

# Nomenclature

| | |
|---|---|
| $\eta$ | Viscosity |
| $\kappa^{-1}$ | Debye length |
| $\mu$ | Chemical Potential |
| $D_{\perp}$ | Diffusion coefficient perpendicular to a wall |
| $D_{\parallel}$ | Diffusion coefficient parallel to a wall |
| $D_h$ | Hydrodynamic diameter |
| $D_{bulk}$ | Diffusion coefficient estimated from Stokes Einstein equation in 80/20 wt.% glycerol/demineralized water |
| $D_{unconfined}$ | Diffusion coefficient estimated from Stokes Einstein equation in 30/70 wt.% glycerol/demineralized water |
| $D_{x,micro}$ | x-component of diffusion coefficient in microchannel |
| $D_{x,nano}$ | x-component of diffusion coefficient in nanochannel |
| $D_{y,micro}$ | y-component of diffusion coefficient in microchannel |
| $D_{y,nano}$ | y-component of diffusion coefficient in nanochannel |
| $f$ | Friction factor |
| $h, z$ | Distance of centre of particle from wall |
| $k_B$ | Boltzmann constant |
| $r$ | Particle radius |
| $T$ | Temperature |
| $u$ | Diffusion velocity |
| $D_{micro}$ | Average value of diffusion coefficient in microchannel |
| $D_{nano}$ | Average value of diffusion coefficient in nanochannel |

# 1

# Introduction

The cellular environment is characterized by confinement and macro-molecular crowding [1, 2]. The impact of cellular environment, on molecular transport and biochemical reactions is not well understood. Both concepts, confinement and crowding, have been studied separately. Hence, there is a need to study biological reactions in an environment that mimics the native environment of cell: confined and crowded simultaneously. This requires an understanding of how molecular transport proceeds in a cellular environment. Nanofluidics provide a platform to create an artificial cell and mimic the cell environment, to achieve the understanding of biological processes. The project carried out caters to meet the first phase of the big picture envisioned: Understanding diffusion in confinement. Hence, the aim of this research is to successfully develop an innovative tool that mimics confinement and study diffusion of an analyte in the same. In the following sections, the relevant theme, current state of the art, research questions, approach and report outline will be discussed.

## 1.1. Relevant Theme

### 1.1.1. Extended nanospaces

Extended nanospaces, defined to be in the size range of 10-1000 nm, have been emerging as an attractive topic of research and extensively investigated. The liquid volume confined in extended nanospaces is comparable to or smaller than that of a single cell volume (few picolitres) [3]. This explains the scope of extended nanospaces to mimic confinement in biological systems. Hence, the aforementioned size range of 10-1000 nm are very often considered in the design of a device mimicking confinement. Moreover, extended nanospaces bridge the gap between a single molecule like behaviour and the bulk behaviour. For instance, the number of water molecules (size of 2.8 Å) in extended nanospaces ranges from 36 molecules (10 nm) to 3600 molecules (1000 nm)[4]. Investigations of molecular transport in this length scale have been carried out, but there exists an ambiguity about the surface effects playing a role (Section 1.2). The ultimate goal of studying molecular transport of biological components and biochemical reactions in a confined crowded system requires to be certain about the liquid properties in the aforementioned size range and the underlying concepts playing a role.

### 1.1.2. Significance of crowding and confinement in biological studies

Biochemical reactions are affected by two different concepts, namely crowding and confinement. Confinement is a static phenomenon[5]. It is volume exclusion by confining boundaries: restricted to cellular compartments/enclosures/pores of comparable dimensions [6]. It affects biological processes. For example, in a study by Wang et. al., it was showed how the nanospace favoured folded state of the enzyme (as in the native cellular environment), leading to higher enzymatic activity. Moreover, laminar flow in the nanochannels enhanced the enzymatic activities due to efficient mixing [7].

Crowding on the other hand is a dynamic phenomenon[5]. It is volume exclusion by the presence of macromolecules (Figure 1.1). The interior of cells is crowded. The macromolecules present inside the

cells take up about 20-30 % of the cell space; which is not available to other components[8]. Crowding also impacts biochemical processes. For instance, it has been showed in a study that the addition of crowding agents lead to structural reorganization of protein leading to smaller sized structures, hence, reducing the propensity of aggregation of proteins[9].

Plenty of studies on both confinement and crowding have been done, but separately. It is difficult to compare the results of two different studies and to arrive at a conclusion [10]. The project carried out is the first step towards achieving the ultimate goal of studying biochemical reactions in a system that is confined and crowded at the same time.

### 1.1.3. Molecular transport in biological cells

The big picture envisioned is the ability to develop a tool to study enzymatic reactions in a confined system and crowded media simultaneously. Using this tool it would be possible to study molecular transport of biological components and kinetics of enzymatic reactions; both as a function of equilibrium and non-equilibrium conditions (temperature, pH, ionic strength, concentration, flow rates). When we speak about molecular transport, it shall be noted that diffusion plays an important role in enzymatic reactions (Figure 1.1).

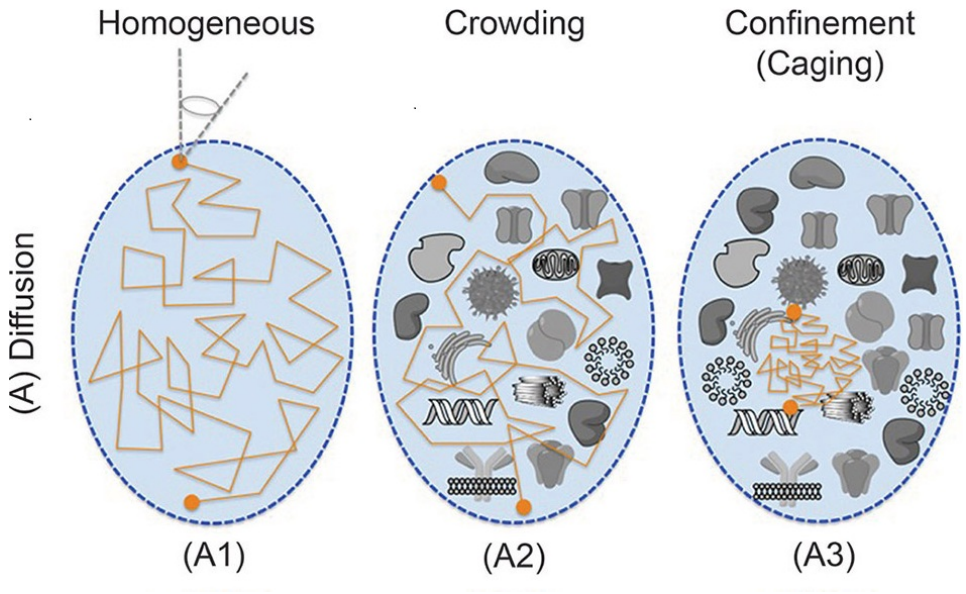


Figure 1.1: Illustration of diffusion (A) in a bulk/homogeneous medium (A1), crowded medium (A2) and confined environment (A3) [11].

The maximum rate of enzymatic reactions is set by the frequency of diffusional encounters of the reactant molecules[12]. The diffusion coefficient of the enzyme and substrate molecule are important parameters, as they affect the magnitude of second order rate constants of enzymatic reactions[13]. Hence, knowing the diffusional behaviour of these molecules in the biological environment (confined and crowded) is of importance. As the first step, we look into diffusion in confinement. Section 1.2 briefly puts light on the current knowledge about diffusion in confinement.

## 1.2. Diffusion in confinement - current state of the art

As already discussed in Section 1.1.3, diffusion of analytes in confinement is relevant to biological systems. Diffusion in confinement is different from diffusion in bulk. This is because diffusion coefficients or the mobility of analytes manifest a different behaviour when going to the nanoscale due to the presence of confining boundaries. Multiple studies have been carried out that attempt to investigate diffusion of analytes in confinement. The reduction of diffusion coefficient of particles in confinement

relative to bulk is related to interaction with the confining walls [14–17]. However, there are conflicting views about the effects of confinement in extended nanospaces on diffusion of analytes. The results reported in literature are not consistent with each other. There is inconsistency in the dependence of diffusion properties of analytes of different sizes in channels of different dimensions. Moreover, there is no agreement between the interpretation of the results that have been reported. Based on the current findings reported in literature, it becomes difficult to predict the anticipated effect of confinement on the diffusion coefficients of analytes in the artificial cell (nanofluidic device) that would be created in this project. The research gap has been further discussed in Section 2.3. Hence, to establish a clear understanding of diffusion in confinement by finding the diffusion coefficient of an analyte in confinement relative to bulk and to bridge the research gap, led to the formulation of research questions as discussed in the following section.

## 1.3. Research Questions

Section 1.2 validates the need to address the ambiguity about diffusion coefficients of solute in nanospace. It is pertinent to draw reliable conclusions about the effect of confinement on diffusion coefficient of analytes relative to bulk and expel the research gap. This led to the formulation of research questions.

To summarize, the research questions to be answered are as listed below:

1. Is the experimental method of determining diffusion coefficient reliable?
2. What is the diffusion coefficient of the analyte found in microchannel / bulk system?
    - Is it the same as the theoretical estimate?
3. What is the diffusion coefficient of the analyte found in nanochannel / confined system?
    - By what magnitude do the confining dimensions of the nanochannel cause the diffusion coefficient of the analyte to deviate from the one found in microchannel?
4. What factors are responsible for yielding the diffusion coefficient as obtained in the nanochannel?
    - What aspects/phenomena pertaining to confinement are relevant to the system under investigation?
    - Explaining the extent of deviation observed from the bulk systems.
5. Can the ambiguity be expelled or research gap filled?

## 1.4. Approach

In the first stage of the project, the design of a tool is proposed which will be self-contained: hybrid micro/nanofluidic device. Such a device allows for a self contained system, wherein one part is expected to behave like a bulk system (microchannels) and the other like a confined system (nanochannels). Investigation of diffusion of an analyte in the same device exhibiting different behavior in the micro and nanochannels will aid in drawing reliable conclusions. Particle tracking method is proposed to find the effective diffusion coefficient of analyte in the channels. The analyte chosen for the study are commercially available polystyrene beads. These beads are 100 nm in size. The size has been carefully chosen to be able to see confinement effects, if any, despite the presence of experimental errors. In order to track the particles in microchannel and nanochannel, the polystyrene beads are dispersed in a mixture of glycerol and water. The Brownian motion of polystyrene beads is then observed in the micro/nanochannel employing Confocal Laser Scanning Microscope. Few preliminary studies are carried out prior to these diffusion coefficient measurements to ensure the reliability and optimization of the method, that will be employed to find effective diffusion coefficients. Thereafter, the analysis of the trajectories obtained from particle tracking then yield the diffusion coefficients of the 100 nm polystyrene beads in microchannel and nanochannel. A comparison is made between the two to draw conclusions about the effect of confinement.

## 1.5. Report Outline

The report consists of 6 chapters. Chapter 1 gives an overview of the motivation behind the project carried out while also stating the goals to be met by the project. Chapter 2 covers relevant theory and findings from literature to give the reader a brief idea of the concepts involved. The chapter also states the current state of the art. Chapter 3 describes the experimental procedures concerning the fabrication of the artificial cell (micro/nanofluidic device), sample preparation (100 nm polystyrene beads suspended in glycerol/water mixture), details of imaging with Confocal Laser Scanning Microscope followed by image and data analysis. The results of the experimental investigation are presented and discussed in detail in Chapter 4. Finally, the conclusions drawn from the work done are presented in Chapter 5 and recommendations are listed in Chapter 6.

# 2

# Theory

This chapter briefly summarizes the concepts involved in answering the research questions. In order to answer the research questions, diffusion coefficient measurements are carried out in two types of system: bulk and confined (microchannel and nanochannel). Hence, in the following sections are described concepts, that are related to diffusion in bulk and confined systems. Sections 2.1.1 and 2.1.2 briefly summarize diffusion in bulk systems from a macroscopic and microscopic point of view. Section 2.2 elaborates on how diffusion gets affected at the nanoscale due to interactions with confining walls. Thereafter, Sections 2.4 and 2.3 put light on the existing research gap when it comes to quantify the effects of confinement on diffusion.

## 2.1. Diffusion in bulk

Diffusion is a long known concept. The most common example would be spreading of a drop of ink inside a bottle of water, which makes it easy to visualize diffusion. In the first part of theory, the phenomena of diffusion is revisited to comprehend several theories that explain diffusion through different approaches.

### 2.1.1. Macroscopic Description

This section addresses diffusion from a macroscopic description throughout a phase. As per the second law of thermodynamics, a uniform spread of matter is expected at equilibrium. This is because the system tends to shift to a state of maximum entropy by spreading throughout the available space [18]. Fick's first law gives the flux of particles, which is proportional to the existing concentration gradient [19]:

$$J = -D\frac{\partial c}{\partial x} \tag{2.1}$$

where $D$ is the diffusion coefficient, $J$ is the flux and $\frac{\partial c}{\partial x}$ is the concentration gradient.

It should be noted that Equation 2.1 is applicable to a one-dimensional system. Using Fick's first law and principles of conservation of mass, is obtained Fick's second law:

$$\frac{\partial c}{\partial t} = D\frac{\partial^2 c}{\partial^2 x} \tag{2.2}$$

Equation 2.2 explains concentration change of a system with respect to time.

If diffusion is explained thermodynamically, the origin of forces is the gradient of chemical potential, $\mu$. Hence, the driving diffusive force, $F_{diff}$ can be written as:

$$F_{diff} = \frac{1}{N_A}\frac{\partial \mu}{\partial x} \tag{2.3}$$

where $N_A$ is the Avogadro's number. Division by $N_A$ is important as $\mu$ is molar quantity. Using the definition of chemical potential, the diffusive force can be re-written as:

$$F_{diff} = \frac{k_B T}{c} \frac{\partial c}{\partial x} \tag{2.4}$$

where $k_B$ is the Boltzmann's constant and $T$ is temperature. Under conditions of stationary state, the force is nothing but force offered by viscous resistance, $fu$. Here, $f$ is friction factor and $u$ is diffusion velocity. Hence, the above equation can be rewritten as:

$$u = \frac{k_B T}{fc} \frac{\partial c}{\partial x} \tag{2.5}$$

Also, the flux of a material through a given cross section should be the product of concentration and its diffusive velocity:

$$J = cu \tag{2.6}$$

Combining Equation 2.6 and 2.5 with Equation 2.1, we get:

$$D = \frac{k_B T}{f} \tag{2.7}$$

When diffusing particles are spherical, the resulting equation is the famous Stokes-Einstein relation:

$$D_o = \frac{k_B T}{3\pi\eta D_h} \tag{2.8}$$

where $\eta$ is the viscosity of solvent and $D_h$ is the hydrodynamic diameter of solute.

It should be noted that Equation 2.8 is derived on the assumption that the solute is moving slowly through a continuum of solvent [20]. It is applicable to fluids of constant density and viscosity, that are in stationary state with laminar flow past a spherical particle.

### 2.1.2. Microscopic Description

Section 2.1.1 treats liquid as a homogeneous system and considers solute to be moving in a soup of liquid. We will now look at the molecular picture of diffusion. Microscopic theory describes diffusion as a result of random motion of molecules or particles. The random motion is a result of kinetic thermal energy ($k_B T/2$ along each axis) associated with the molecules. Hence, a solute molecule dispersed in a liquid often bumps into the molecules of liquid [21]. Such random thermal fluctuations cause the solute to wander around, which is famously called Brownian motion. It has been named so after Robert Brown, who was the first to observe the random motion of pollen grains in 1827. To explain the Brownian motion, let us consider one dimensional random walk as given by the Einstein-Smoluchowski theory [21, 22]. The rules concerning the aforementioned one dimensional random walk are as mentioned below:

- Each particle takes a step $l$ every $\tau$ seconds either to the left or right.
- The probability of going to the right or left is equal and is 1/2.
- The movement of each particle is independent of the other.

In one dimensional space, let us assume the probability of a particle going right to be p. Then the probability of going left is 1-p. Hence, using the binomial distribution, the probability of a particle taking k steps to the right in n number of trials can be given by:

$$P(k) = \frac{n!}{k!\,(n-k)!} p^k (1-p)^{n-k} \tag{2.9}$$

For a large value of n, Equation 2.9 reduces to a Gaussian distribution, resulting in the following equation:

$$P(x)dx = \frac{1}{\sqrt{4\pi D t}} e^{\frac{-x^2}{4Dt}} dx \tag{2.10}$$

The above equation is the probability of finding a particle between the region x and x+dx. The standard deviation of the above equation is $\sqrt{2Dt}$. This results from the defining the diffusion coefficient to be $l^2/2\tau$ . We see that the distribution forms a bell shaped curve (Figure 2.1). It shall be noted that 68% of the diffusing species falls within one standard deviation of the Gaussian curve. The probability of the diffusing molecule travelling further away from this region would be 0.32, 0.045 if it travels twice the standard deviation or 0.0026 for a distance thrice the standard deviation.

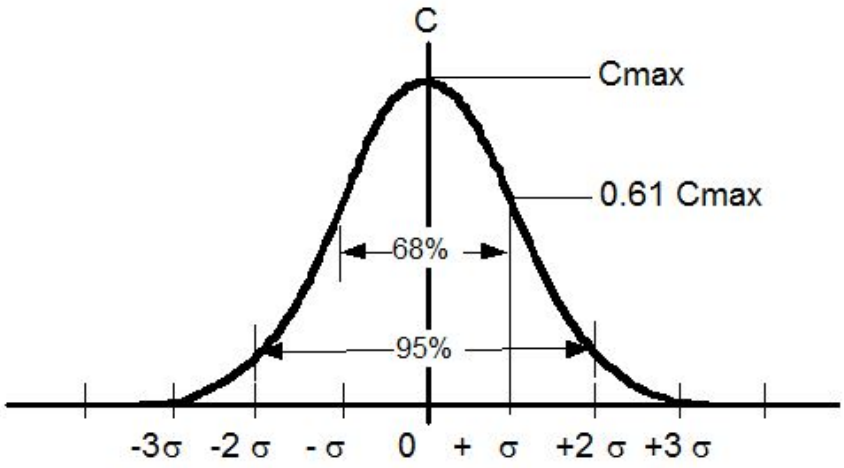


Figure 2.1: Distribution of a diffusing species from a point source forming a bell curve. At any given instant of time, 68% of the population falls within $\pm\sigma$, 95% within $\pm 2\sigma$ and 99.7% within $\pm 3\sigma$[23].

Hence, we see how a microscopic description of the system links us to the macroscopic property of diffusing species. While diffusion coefficient can be obtained from the famous Stokes-Einstein relation (Equation 2.8), it can also be obtained from using a microscopic property (step length) of the system under investigation. Understanding diffusion in bulk, let us see now see in the following section what factors play a role in changing the diffusion behaviour when going to nanoscale.

## 2.2. Diffusion in Confinement

The significance of confinement to enzymatic reactions has already been mentioned in Section 1.1.2. The relevance of confinement is however not just limited to biochemical reactions, but extends to a diverse field such as surface chemistry, membrane and separation science and, soil science, to name a few [24]. When going to smaller channels in the submicron or nano range, has natural consequences [25]. This is related to the increase in specific interface area as the channel size is reduced. Interactions with the surface become a key factor and liquid properties are expected to change. Viscosity may not be constant throughout, as assumed in the derivation of Stokes-Einstein equation. Several other forces affect the movement of solute through the solvent. In the following subsections, different phenomena relevant to nanoconfinement have been discussed. These are namely hydrodynamic interactions (Section 2.2.1), role played by the electrical double layer and Van der Waals forces (Section 2.2.2) and increased viscosity (Section 2.2.3). These will help us understand how diffusion behaviour of analytes is affected at the nanoscale.

### 2.2.1. Hydrodynamic Interactions

Hydrodynamic forces, relevant to colloidal systems, are forces that are generated by relative particle fluid motion[26]. When a particle moves in a fluid, it creates a disturbance or flow field around itself. These disturbances are long range interactions that travel via the solvent. If there is a wall or another particle at a finite distance, these disturbances affect/damp the movement of the particle. Such effects

are relevant to systems with very low Reynolds number, where viscous forces dominate over inertial forces [27].

When a particle, of radius *r*, is moving freely in a solvent of viscosity, $\eta$, it experiences a drag force that acts opposite to its direction of velocity ($\vec{U}$). Under the condition of low Reynolds number, this drag force can be given by Stoke's law [26]:

$$F_D = -6\pi\eta r\vec{U} \tag{2.11}$$

This is the drag force that results due to relative motion of particle with respect to the fluid [22]. This ultimately results in obtaining the diffusion coefficient prescribed by the famous Stokes Einstein relation (Equation 2.8). However, when there is an obstacle present in the vicinity of a particle, the diffusion coefficients deviate from the Stoke's equation (Equation 2.8). Let us now look at the analytical solution/prediction that is proposed in literature to find the effective diffusion coefficient when it is trapped between two parallel walls (which is the case relevant to the work done in this project). It is famously called the method of reflection [28], which is now further discussed.

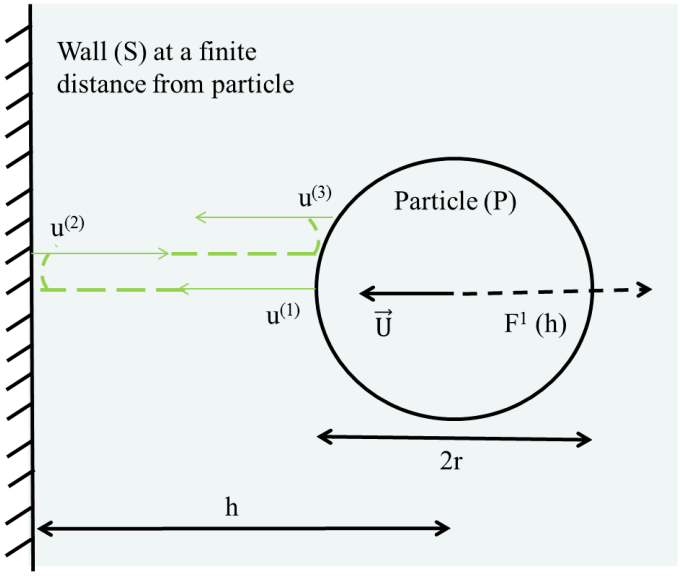


Figure 2.2: Drag force F acting on a particle of radius r, moving with a velocity U. There is a rigid wall S at a distance h from the centre of the particle. The velocity fields used in the expansion are represented by dashed green lines.[28].

Method of reflection is based on the idea of determining the flow field in an iterative way. The flow field originating from a particle is virtually reflected from the wall present at a finite distance and further bouncing back from wall to the particle. This results in a series of corrections to the flow field due to the presence of an obstacle (Figure 2.2)[27]. In the proposed analytical solution [28], the usual boundary conditions apply:

$$\begin{aligned} \vec{u} &= \vec{U},\ on\ P \\ \vec{u} &\to 0,\ at\ infinity \end{aligned} \tag{2.12}$$

If an obstacle, wall *S* (Figure 2.2) is present at a finite distance from a particle *P*, then the velocity field must vanish at the surface of the obstacle. Because of the linearity of the Stoke's equation, the velocity $\vec{u}$ and pressure *p* of the fluid can be written as a sum of fields:

$$\begin{aligned} \vec{u} &= \vec{u}^{(1)} + \vec{u}^{(2)} + \vec{u}^{(3)} + \vec{u}^{(4)} + .... \\ p &= p^{(1)} + p^{(2)} + p^{(3)} + p^{(4)} + ... \end{aligned} \tag{2.13}$$

Each pair of $\vec{u}$ and *p* can be determined by the application of boundary conditions as mentioned

below (refer to Figure 2.2):

$$\begin{aligned} \vec{u}^{(1)} &= \vec{U},\ on\ P \\ \vec{u}^{(2)} &= -\vec{u}^{(1)},\ on\ S \\ \vec{u}^{(3)} &= -\vec{u}^{(2)},\ on\ P \\ \vec{u}^{(4)} &= -\vec{u}^{(3)},\ on\ S \end{aligned} \tag{2.14}$$

Under such conditions, it is ensured that the physical conditions met by the resultant velocity are proper; that is:

$$\begin{aligned} \vec{u} &= \vec{U},\ on\ P \\ \vec{u} &= 0,\ on\ S \\ \vec{u} &\to 0,\ at\ infinity \end{aligned} \tag{2.15}$$

The velocity of the moving particle is affected by a factor of *r/h*, where *h* is the distance of the centre of the particle from the wall. Hence,

$$\begin{aligned} \vec{u}^{(3)} &= O\left(\frac{r}{h}\right)\vec{u}^{(1)} \\ \vec{u}^{(5)} &= O\left(\frac{r}{h}\right)\vec{u}^{(3)} = O\left(\frac{r}{h}\right)^2\vec{u}^{(1)} \end{aligned} \tag{2.16}$$

The drag force that acts on the particle is the sum of drag force contributed by the odd numbered fields (Figure 2.2). Hence,

$$F_{drag} = F^{(1)} + F^{(3)} + F^{(5)} + \ldots \tag{2.17}$$

In the absence of an external obstacle, only the first term remains and results in the drag force acting on an unbounded particle, as given by the Stoke's equation. A similar method of reflection is extended to a system wherein a particle is trapped between two walls, wherein the velocity disturbance traverses from the particle to meet the first wall and then bounces on the second wall that pushes the particle in the same direction as its velocity.

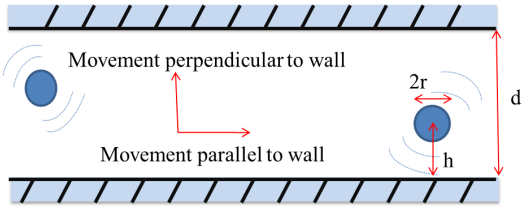


Figure 2.3: Particle trapped between two walls and executing Brownian motion.

Hence, for a particle bounded between two confining walls (Figure 2.3, the drag force can be written with a slight modification of the Stoke's law [29]. The parallel and perpendicular components of the drag force can be written as:

$$\begin{aligned} F_\perp &= -6\pi\eta r\vec{U}\lambda_\perp = \lambda_\perp F_D \\ F_\parallel &= -6\pi\eta r\vec{U}\lambda_\parallel = \lambda_\parallel F_D \end{aligned} \tag{2.18}$$

This implies that the modified equation for diffusion coefficients would now be:

$$\begin{aligned} D_\perp &= \frac{k_B T}{6\pi\eta r\lambda_\perp} = \lambda_\perp^{-1} D_o \\ D_\parallel &= \frac{k_B T}{6\pi\eta r\lambda_\parallel} = \lambda_\parallel^{-1} D_o \end{aligned} \tag{2.19}$$

In the equations above, $\lambda_\perp$ and $\lambda_\parallel$ are the correction factors. The solution for the same have been found and reported[29]. $\lambda_\perp$ has an exact solution (reported by Brenner [30]) while $\lambda_\parallel$ has an approximate solution:

$$\lambda_\perp^{-1} = \frac{D_\perp}{D_o} = \frac{4}{3}\sinh(\alpha)\sum_{n=1}^{\infty}\frac{n(n+1)}{(2n-1)(2n+3)}\left[\frac{2\sinh((2n+1)\alpha)+(2n+1)\sinh(2\alpha)}{4\sinh^2((n+1/2)\alpha)-(2n+1)^2\sinh^2(\alpha)}-1\right] \quad (2.20)$$

where $\alpha$ is $\cosh^{-1}$(h/r).

$$\lambda_\parallel^{-1} = \frac{D_\parallel}{D_o} \approx 1 - \frac{9}{16}\left(\frac{r}{h}\right) + \frac{1}{8}\left(\frac{r}{h}\right)^3 - \frac{45}{256}\left(\frac{r}{h}\right)^4 - \frac{1}{16}\left(\frac{r}{h}\right)^5 \quad (2.21)$$

The approximate solution of $\lambda_\parallel$ (Equation 2.21) holds good only for h/r $\gtrsim$ 1.5. This is because method of reflection fails to produce accurate results for smaller separations. The closer a particle approaches a wall, the number of reflections increases and higher order approximations are required to yield reliable results [27]. In another study, a solution obtained from a different approach (using lubrication method at smaller separations, that takes into account the strong velocity gradients between the small space) has been proposed for predicting mobility parallel to confining walls [31]. It has been found to be more accurate for smaller values of h/r and is given by:

$$\left(\frac{D_\parallel}{D_o}\right)^{-1} \approx 1 - \frac{8}{15}\ln\left(1-\frac{r}{h}\right) + 0.029\left(\frac{r}{h}\right) + 0.04973\left(\frac{r}{h}\right)^2 - 0.1249\left(\frac{r}{h}\right)^3 \quad (2.22)$$

Moreover, the exact solution for $\lambda_\perp$ (Equation 2.20) is an infinite series, and makes it quite inconvenient for reference solution. Hence, a good approximation for the same has been proposed, that is obtained by regression method [31]:

$$\lambda_\perp^{-1} = \left(\frac{D_\perp}{D_o}\right) \approx \frac{6 - 10(r/h) + 4(r/h)^2}{6 - 3(r/h) - (r/h)^2} \quad (2.23)$$

The aforementioned approximations have been quite often used to predict the impact of hydrodynamic interactions of the diffusion behaviour of a solute close to a wall. For instance, a group of researchers investigated the diffusion coefficients of polystyrene beads, 1 $\mu$m in diameter, suspended in a system of deionized water with 10 mM of NaCl. They found the diffusion coefficients parallel and perpendicular to a rigid wall using the [32].

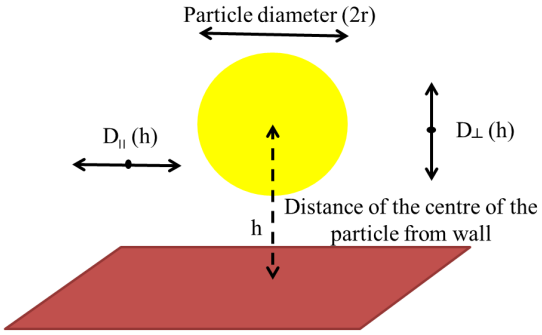


Figure 2.4: Schematic representation of the two components (parallel and perpendicular) of diffusion coefficients close to an obstacle. The distance of the centre of the particle from the wall (h), affects $D_\parallel$ and $D_\perp$ [32].

The analytical predictions of the results were obtained using Equation 2.22 for $D_\parallel$ while they employed Equation 2.21 to find $D_\perp$. They reported the experimental results to have good agreement with the theoretical predictions as discussed in Section 2.2.1 (Figure 2.5). It was observed that the effective diffusion coefficient of the particle decreased due to the presence of an obstacle close to a particle executing Brownian motion. Moreover, the movement of particle perpendicular to the wall was impeded more than the mobility of the particle parallel to the wall. A similar scenario can be encountered in a nanochannel. If the solute is large enough and confined between the walls of nanochannels, hydrodynamic interactions can affect its mobility.

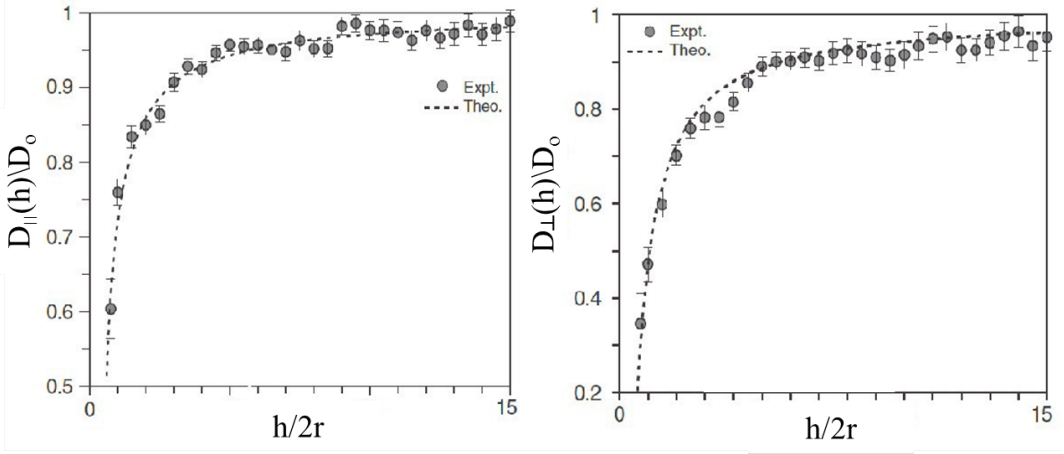


Figure 2.5: Left: Diffusion coefficient of 1 $\mu$m polystyrene bead parallel to a rigid wall. Right: Diffusion coefficient of 1 $\mu$m polystyrene bead perpendicular to the rigid wall. As clear from the experimental and analytical results, the impact of the presence of a wall is more on perpendicular component of diffusion coefficient than on the parallel component. [32].

### 2.2.2. Forces acting at the nanoscale

In the preceding section was discussed how the presence of confining walls at a finite distance from a particle can affect its mobility due to hydrodynamic interactions. Several other types of forces play a role at the nanoscale. These forces can give rise to different equilibrium phenomena (varying distribution of ions) or kinetic phenomena (viscosity changes), which have an impact on diffusion behaviour [24].

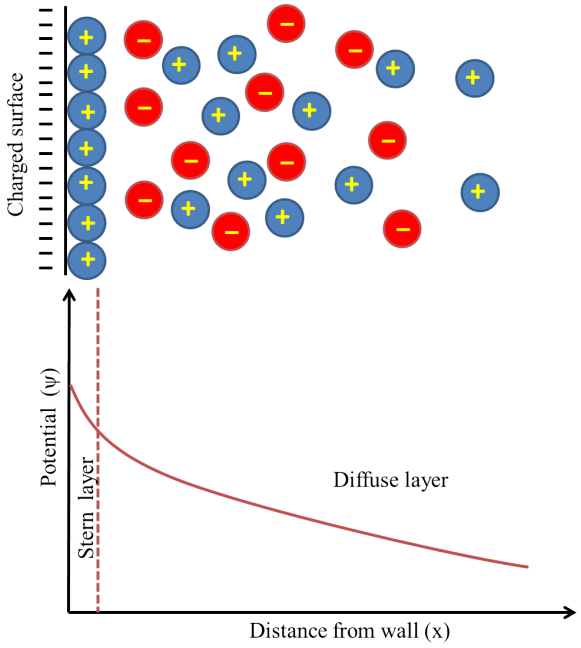


Figure 2.6: Schematic representation of double layer formation at a solid liquid interface.

In a system containing ions and a charged interface, the density of ions near the surface varies [18], which is known as electrical double layer. At the solid-liquid interface, oppositely charged ions form a layer which is called the Stern layer. The ions in this layer are assumed to be adsorbed at the surface. Beyond the Stern layer, is the diffuse layer, where the charge distribution is such that a profile for the electric potential follows the trend as depicted in Figure 2.6. The thickness of this double layer, called the Debye length ($\kappa^{-1}$), is given by:

$$\kappa^1 = \left( \frac{4\pi e^2 N_A}{1000 \varepsilon k_B T} \sum_i z_i^2 M_i \right)^{1/2} \tag{2.24}$$

where $e$ is unit positive charge, $N_A$ is Avogadro's number, $\varepsilon$ is dielectric constant of medium, $z_i$ is the valence number and $M_i$ is the molar concentration of component i.

From Equation 2.24, it can be seen how the thickness of double layer varies inversely the electrolyte concentration. In a nanochannel, the thickness of the double layer has an impact on the Brownian motion of particles. In most actual cases, the thickness of double layer lies in the range of 1 nm to 100 nm [33]. In confined systems, there can be situations where an electrical double layer overlap can be encountered or the the thickness of double layer might be much smaller than confining dimensions.

The formation of a double layer in confined systems has implications on the movement of solute molecules. If a system has similarly charged particles and walls, what can be expected? High ionic strength results in a thin double layer, which does not prevent the particle interacting with the walls, as a result of which the effective diffusion coefficient deviates from bulk value significantly (Figure 2.7). When the double layer thickness increases, the number of particles interacting with the walls is negligible and the extent of deviation from bulk diffusion coefficients decreases. However, when the double layer is large enough but not overlapping, the interaction with the walls is dominant again, decreasing the diffusion coefficient significantly. This behaviour of particles in nanochannel with electrical double layer was confirmed by Durand et. al.(2009) who investigated diffusion of negatively charged proteins in nanochannels that were 50 nm high, 10 $\mu$m wide and 30 $\mu$m long. The walls of the nanochannel were also negatively charged [34].

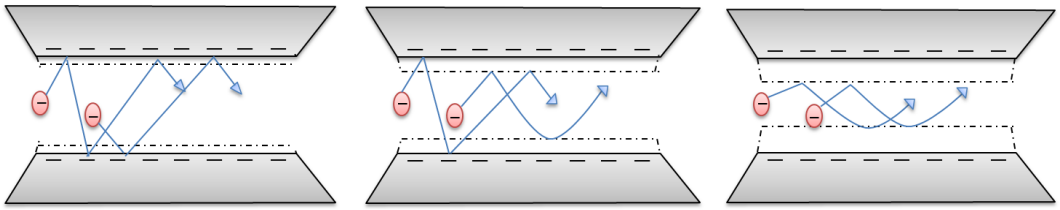


Figure 2.7: Schematic representation of double layer formation in a nanochannel. The surface and particle both are similarly charged. (a) When the double layer is very thin, the interaction of particles with the walls is not prevented. This results in reduced diffusion coefficients of the particles. (b) For slightly thicker double layer, the number of particles interacting with wall reduce. (c) When the double layer is thick enough particles do not interact anymore with the walls of the nanochannel[34].

A similar observation was made in an attempt to understand the implications of double layer formation, smaller in size than the particle size[35]. 1 $\mu$m polystyrene beads were suspended in deionized water and its interaction with glass surface was studied. Varying concentration of NaCl was used in the investigation to get a range of Debye length thickness ( 1.4 nm - 4.3 nm). An approximate analysis of the average position of the particle from the surface was presented. The interaction energy between the particle and a surface with double layer is given by:

$$P_{DL}(S) = Ae^{-S/\kappa^{-1}} \tag{2.25}$$

where, $S = h\text{-}r$, with $h$ as the distance of the centre of the particle from the wall and $r$ as the particle radius, $A$ is a constant dependent on surface potential and $\kappa^{-1}$ is the Debye length.

Gravitational potential energy for the particle can be given by:

$$P_G(S) = \frac{4}{3}\pi r^3 (\rho_P - \rho_L) g S \tag{2.26}$$

Where $g$ is acceleration due to gravity, $\rho_P$ and $\rho_L$ are the densities of the solute and solvent respectively. Hence, the total potential energy of the particle becomes:

$$P(S) = Ce^{-\left[P_{DL}(S)+P_G(S)\right]/k_BT} \tag{2.27}$$

where *C* is a normalization constant.

Using Equation 2.27, the average position ($S_o$) of the particle as a function of Debye length can be found such that $\left[(d/dS)(U_D L(S)+U_G(S))\right]_{S_o}$=0. In considering Equation 2.27, Van der Waals interactions have been neglected. The investigation led to the result that as the thickness of double layer decreased with increasing salt concentration, the particle approached closer to the glass surface. This reflected in the reduced values of the parallel component of the diffusion coefficient ($D_{parallel}$), with increasing salt concentration. This was explained as the repulsion between surface and the particle due to the presence of an electrolyte, that formed a double layer.

Hence, we see that how the presence of a double layer might act as a reflecting wall and result in a more favourable distribution of particles inside a channel. Such a distribution of particles inside the nanochannels in turn have an impact on the effective diffusion coefficient of the particle that is observed. Furthermore, special cases might be encountered where the solute diffuses through a system of strongly overlapping electrical double layer. In such a case electroviscous effects have been found to hinder the particle movement more severely[36]. When a particle in a nanochannel moves due to thermal agitation, the ions in the diffuse layer of the electrical double layer are dragged along with its motion. This is the electroviscous effect that is known to retard the motion of solute [37].

Several other forces come into play when going to even smaller length scales in the nano range. These forces can be attributed to inter molecular forces between two surfaces. Van der Waals attractive interactions are a result of interaction due to induced dipoles, originating from random fluctuations in charge distribution around molecules [33]. The typical length scales of such interactions is 1-10 nm [17]. At close separations (a few nm), Van der Waals attractive forces dominate over the repulsive electrical double layer forces, which causes a net attractive force. When a particle is close to a surface, it feels attractive forces due to Van der Waals interactions and at the same time is repelled by the electrical double layer. There is competition between the two forces. When particles are diffusing in confined channels interacting with walls and other particles due to random Brownian motion, then at very close separations Van der Waals forces might cause sticking or agglomeration.

However, at closer separations few other forces apart from Van der Waals forces come into picture. With confinement, interaction of particles with the walls of the confining boundary and other particles is the system increases having an impact on the stability of the system [38]. Hydration and hydrophobic interactions start to play a role when a particle is in close proximity to a surface [33]. Hydration forces are short range repulsion forces. It relies on the hydrogen bonds formed with water and other molecules. It comes into picture when two hydrophilic surfaces are brought close to each other, resulting in a repulsive force. Hydrophobic interactions on the other hand is a force of attraction resulting from interaction between hydrocarbons. It is associated with the rearrangement of water molecules around hydrophobic molecules or the structural rearrangement of water when two hydrophobic solute molecules approach each other. Hydration forces between surfaces act on a length scale of around 5 nm while hydrophobic interactions are relevant on a length scale below 8 nm. At smaller separations hydrophobic interactions can dominate over Van der Waals attractive forces[38]. Hydrophobic and hydration interactions become more important especially when studying biological systems [17]. Such forces affect the stability of solute inside closely confining channels and could also be the reason for adhesion to the walls or agglomeration of particles.

### 2.2.3. Layering and Increased Viscosity

The increasing surface to volume ratio in nanochannels, also has an impact on liquid properties. Changing liquid properties are expected to change the mobility of solute through the same.

A consequence of going to the nano scale is found to be the layering of liquid at the surface. This is because of the increased surface and molecule interactions leading to inhomogeneous fluid

density profile inside nanochannels. It has been found that the packing density and viscosity of fluids in nanochannels close to the wall are different from the bulk value (Figure 2.8)[39].

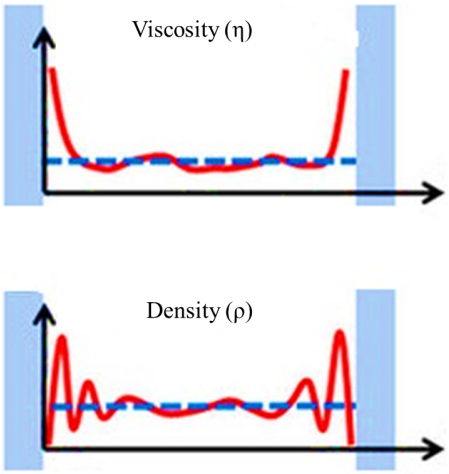


Figure 2.8: Schematic representation of density and viscosity variations of fluid as a function of distance from the walls (blue) of a nanochannel as a result of molecular surface effects. Blue dashed line is indicative of bulk value while the red line is the observed value of density and viscosity in the nanochannels. [39].

For instance, in a study was investigated the effect of nanoconfinement on the properties of water [40]. Atomic force microscopy was employed to determine the layering and increased viscosity of water. It was found that wettability of surface played an important role in altering the water properties. Density profiles for water attained bulk values beyond a gap width of 1.2 nm. Strong layering was observed near the walls of a wetting surface upto a distance of few Angstrom. Layering was also observed when water was in the contact of a non wetting surface, but different in nature from that observed for layering in the case of a wetting surface. The amplitude of increased density seen in the case of a non wetting surface was less than that observed for water on a wetting surface. Viscosity of water was also measured. When the confining surface was wetting (glass and mica), a viscosity increase of about 4 times the value of bulk was observed near the surface. However, bulk viscosity of water was recovered at a distance of about 2 nm from the surface. While, for a non-wetting surface(graphene), the viscosity of water was not found to be affected by the degree of confinement and retained its bulk value all throughout. The dependence of the extent of viscosity increase on the material of the wall was also confirmed in another study by Rudyak et.al. (2011) [41]. Hence, an insight into changing water properties at the nanoscale suggest that increased viscosity in nanochannels as a result of interactions of the solvent molecules with the wall can retard the diffusion of solute through the solvent.

## 2.3. Investigations on Diffusion in Confinement

In the preceding sections, it was discussed how diffusion is affected by the presence of additional forces in the nanochannel as compared to bulk. To quantify the extent of deviation of diffusion coefficients of solute in nanochannels from bulk systems, several investigations have been carried out. This section summarizes few findings from literature while also emphasizing on the existing research gap.

Pappaert et. al.(2005) measured molecular diffusion coefficients for DNA molecules of different sizes. The radius of gyration ($r_g$) of DNA molecules was in the range of 1.9 - 3.8 nm. Measurements were carried out in channels of varying depth (in the range of 18 $\mu$m to 260 nm) and width of 700 $\mu$m. Measurements in channels of depth upto 1.5 $\mu$m yielded values of bulk diffusion coefficient as expected. However, a decrease in the effective diffusion coefficient was observed when the channel depth became smaller than 1 $\mu$m. For DNA molecules with $r_g$ of 1.9 nm in a channel of height 260 nm, a mobility decrease of about 32% was observed. The size of DNA molecules corresponded to 1-3 % of the channel height of 260 nm. The observed slower diffusion was attributed to the presence of walls. It was concluded that wall effects can no longer be neglected when the channel size goes below

a critical value(in their experiments below a depth of 1 micron) [42]. The conclusion drawn from the study does not specifically attribute the reduction in diffusion coefficients to a cause factor, i.e. what kind of interactions could be playing a role? If the size of solute is compared to the channel size, it is unlikely that hydrodynamic interactions play a role in retarding the mobility of solute. Was it then the presence of an overlapping double layer or increased solvent viscosity? The questions remained unanswered.

Hoang et. al. (2011) investigated diffusion of 25 nm quantum dots in channels that were 20 $\mu$m wide and 150 nm high. The results of their experiments was an effective diffusion coefficient 3 times smaller than the bulk value of diffusion coefficient. Hydrodynamic interactions slow down the effective diffusion coefficient only by approximately 12%, as per their speculation. It was speculated that viscosity effects being localized to distances of 1-2 nm, do not contribute to an increased bulk viscosity and therefore do not play a role in affecting the mobility of the solute. The impact of electroviscous effects was also evaluated. A decrease of about only 10% in diffusion coefficient was expected. Hence, that failed to explain the extent of reduced mobility they observed in their experiments. It was concluded that there seems to be a lack of theory to explain their results[37].

On the contrary, Kaji et. al.(2006) attributed their results to increased viscosity of water in nanochannels. They investigated diffusion of 50 nm carboxylate modified polystyrene spheres, dispersed in distilled water, in channels that were 400 nm high. The reduction in observed diffusion coefficient as compared to bulk value of diffusion coefficients was $\sim$68%. It was concluded that the resulting reduced mobility of the particle was observed due to increased viscosity of solvent in the nanochannels [43].

Viscosity changes reported by Li et. al.(2012), were yet again contrasting from what was reported by Kaji et. al and Hoang et. al [44]. Li et.al. studied the viscosity of water in plate and square nanochannels. Square nanochannels had width(W) and depth(D) in the nano range while the plate nanochannels had width in the micro range while depth in the nano range. They reported significant bulk viscosity increase for square nanochannels. Plate nanochannels also showed an increase in viscosity but only for channels with depth less than 200 nm. As per the conclusions drawn from this study, Kaji et. al. should not have encountered bulk viscosity increase, while Hoang. et. al. could have expected an apparent increased bulk viscosity. Li et. al. attributed this effect to the adsorbed layer of water molecules on glass surface. They reported that this layering of water extends to about 24 nm from the wall of the channel for square nanochannels. For plate nanochannels, the layer extends to only about 0.4 nm but appears as an increased bulk viscosity for channels smaller than 200 nm. It was further concluded that electroviscous effect can be rejected as a cause for apparent increased viscosity.

The conclusions drawn by Li et. al. was further in contradiction with Tas et. al.(2004), who examined fluid properties in rectangular microchannels that were 1 cm long, 20 $\mu$m wide and high in the range of 50-150 nm. It was reported that viscosity of demi water increases significantly for all channel sizes. They attributed this effect to electro viscous effect causing over lap of double layer, and not ordering of water molecules at the surface, as that extends only to a few monolayers. They speculated the ionic content in demi water coming from the dissociation of dissolved $CO_2$ to yield a double layer. Conductivity testes yielded concentrations of the ions that would give a Debye length of 0.2 $\mu$m. Viscosity experiments were repeated for 0.1 M NaCl solution and it was found that the apparent viscosity became the same as bulk viscosity for all channel designs. This was attributed to high salt concentrations suppressing the streaming potential[45].

Hence, it becomes evident that there is no agreement between the results of studies that have been reported. It is pertinent to know what kind of effects play a role in hampering the mobility of an analyte in a solvent through a nanochannel and mention distinctly the contributing factors - whether it is the hydrodynamic interactions, presence of a double layer or solvent viscosity increase?. As per the summary of few studies discussed above, it becomes difficult to anticipate the kind of effect/extent of retardation that would be seen if the mobility of an analyte was investigated in the tool that will be designed and fabricated in this project. Hence, this led to the formulation of research questions.

Table 2.1: Summary of diffusion coefficient investigation results reported in literature.

| Author | Details of system under investigation | Results reported | Conclusion drawn |
|---|---|---|---|
| Pappaert et. al. (2005) | Diffusion coefficients molecules of size 1.9-3.8 nm investigated in 18 $\mu$m-260 nm deep channels | 32% decrease in diffusion coefficients relative to bulk | Wall effects below 1 $\mu$m become noticeable |
| Hoang et. al. (2011) | Diffusion coefficient of 25 nm particles found in 150 nm high channels | 67% decrease in diffusion coefficients relative to bulk | Hydrodynamic interactions (12%) and electroviscous effects (10%), No concluding remarks |
| Kaji et. al. (2006) | Diffusion coefficient of 50 nm particles found in 400 nm high channels | 68% decrease in diffusion coefficients relative to bulk | Increased solvent viscosity |
| Li et. al. (2012) | Investigated viscosity in plate and square nanochannels | Bulk viscosity increase for channels only smaller than 200 nm | Layering of water molecules |
| Tas et. al. (2004) | Investigated viscosity in 50-150 nm deep nanochannels | Bulk viscosity increase for all channels | Electroviscous effects responsible and not layering of water molecules |

## 2.4. Research Gap

Section 2.3 encapsulated few examples from literature that aimed to cast light on current knowledge of behaviour of fluid or analytes in confinement. The presence of a research gap becomes evident in the following sense:

- Inconsistency among results.
- Evaluation of the effect of confinement attributed to factors, not agreeing with each other in different studies.
- Obscure size dependency.

Hence, it becomes important to clear the confusion. Following the investigations reported in literature it became difficult to predict what kind of an effect will be seen for the artificial cell (hybrid micro/nano fluidic device) that will be made in this project to cater to the ultimate goal. Hence, this led to the formulation of the research goal ”Study of Diffusion in Confined Nanospace”. In order to draw reliable conclusions from this study, the first step was to experimentally find the diffusion coefficient in bulk system (microchannel) and use it as a reference. This was followed by diffusion coefficient measurements in confined system (nanochannel). The results obtained were further analyzed through different lenses, compared to other studies that have been reported and an attempt to expel the ambiguity was made.

# 3

# Experimental Methods

In this chapter, the materials and methods used to experimentally obtain the diffusion coefficients of solute in microchannel and nanochannel have been discussed. The first section lists all the chemicals that have been used. Section 3.2 describes the step by step fabrication of the hybrid micro/nanofluidic device. The preparation of samples and tracking of particles in the channels using Confocal Laser Scanning Microscope (CLSM) has been described in Section 3.3. A brief description of the principle of working of confocal microscope has also been presented. Section 3.4 gives the details of how the image analysis and data analysis is done to obtain the diffusion coefficient data.

## 3.1. Materials

Potassium Chloride (KCl), Ethanol, Isopropyl Alcohol (IPA), Cyclopentanone, Trichloro silane (1H,1H,2H,2H-perflurooctyl) and Glycerol 99% were obtained from Sigma Aldrich. FluoSpheres Carboxylate-Modified Microspheres, 100 nm, red fluorescent (580/605) was purchased from Thermofisher. SU8 2005 photoresist and 1-methoxy-2-propyl acetate (SU8 developer) were obtained from MicroChem. Polydimethylsiloxane (PDMS) base and curing agent(Sylgard® 184 Silicone Elastomer Kit) was purchased from Dow Corning Corporation.

## 3.2. Device fabrication

Fabrication of the hybrid micro/nanofluidic device involved three stages. In the first stage, the design of the channels was created using a software package. Thereafter, using the design, pattern was optically transferred to a substrate using photolithography. The substrate with the pattern then functioned as a master using which the third step of fabrication, soft lithography, was performed to obtain the final device.

### 3.2.1. Designing of mask

The first step in device fabrication is designing a mask. Photomasks are usually templates of glass, coated with chrome, and are used to optically transfer patterns onto a substrate [46]. The pattern to be transferred are the nanochannels and microchannels, which first need to be designed using a drawing software package. The channels were designed to be of H-shape(Figure 3.1). The horizontal channel was the nanochannel while the vertical legs flanking the ends of the nanochannel were designed to be the microchannels. A design of this form was proposed as this would serve the purpose of ultimate goal of studying enzymatic reactions in the nanochannel as a function of equilibrium and non-equilibrium conditions. Hence, such a design allows to maintain similar and dissimilar conditions of pH, temperature, concentration and velocity of fluid at the two ends of nanochannel. However, to meet the research goals of current study, the requirement was to ensure that the nanochannel was filled with solvent and a few solute particles of interest.

Table 3.1: Channel design specifications.

| | Length | Width | Depth |
|---|---|---|---|
| Microchannel | few millimeters | 200 $\mu$m | 5 $\mu$m |
| Nanochannel | 15,50,30,100,150,200 $\mu$m | 5,10 $\mu$m | 500 nm |

The proposed dimensions of the channel are as listed below in Table 3.1. The depth of the nanochannel was chosen to be 500 nm, which lies in the range of 10-1000 nm (extended nanospace), as discussed in Section 1.1.1.

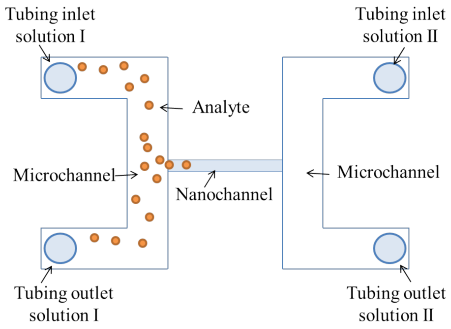


Figure 3.1: Top view of the design of the hybrid nano/microfluidic device. The nanochannel is flanked on its end by microchannels. Analyte injected into the microchannel diffuses into the nanochannel.

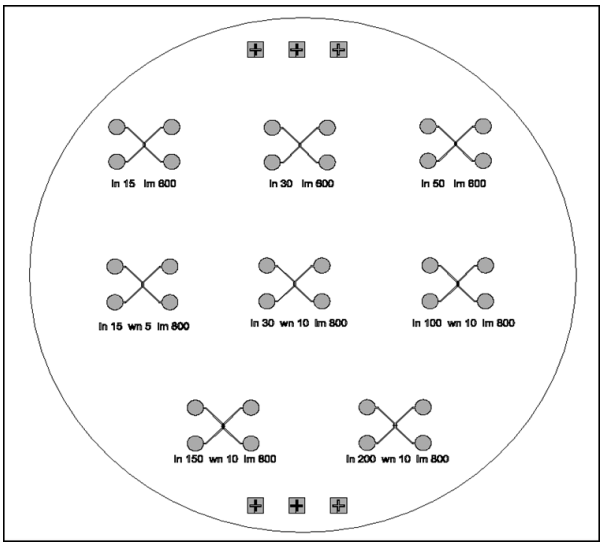


Figure 3.2: Mask design created using the software tool Ledit. The figure depicts the layout of the channels on a substrate of size 4 inch (the circle).

The channels were designed using the software L-edit (Version 16.3) for a substrate of 4 inch (Figure 3.2). Two masks were designed wherein one layer corresponded to the microchannels and the other to the nanochannels (Figure 3.3). The three symbols present in a line at the top and bottom of the design in Figure 3.2 are called markers. Markers are essential to align the layer of microchannels to nanochannels so as to be able to get the nanochannels at the desired location with respect to microchannels.

Since, the substrate size was 4 inch, the mask was required to be 5 inch $\times$ 5 inch. Other specifications of the glass mask were DF (dark field) and CDRR (Chromuium Down Right Reading) [47]. Dark field implies that the channels in grey and red colour would be transparent on the glass while the rest of the regions in the mask would be opaque, coated with chromium. CDRR on the other hand ensures

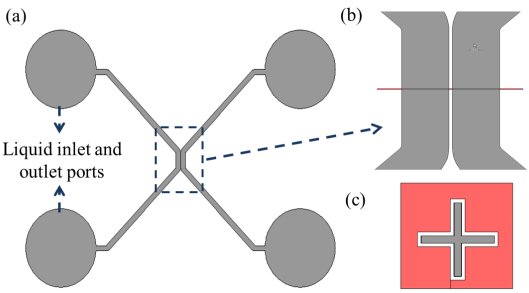


Figure 3.3: The elements present on the mask consist of two layers: microchannel and nanochannel. (a) The hybrid micro/nanofluidic device with the microchannels (grey colour) and liquid injection and outlet ports. (b) Magnified view of the central portion of the device where the nanochannel is present (red colour). (c) Markers designed on both the layers (red and grey) for the purpose of alignment.

that, the substrate gets the pattern in the same way as it appears in the design file. The mask was printed by DeltaMask.

### 3.2.2. Photolithography

Photolithography is the next step, after designing of mask in the process of device fabrication. It is the process of using light to transfer pattern onto a substrate [48]. The substrate used was silicon wafer. This step of device fabrication was performed in a cleanroom (Kavli Nanolab, Delft). It involves a series of processes which were performed first for nanochannel patterning followed by the repetition of the sequence for microchannel patterning. In the following paragraph, the steps and process conditions for nanochannel patterning have been described.

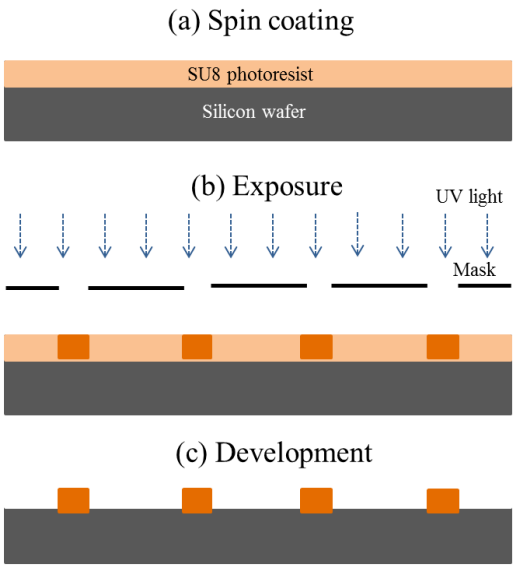


Figure 3.4: Schematic overview of the process of photolithography. SU8 negative photoresist was spin coated onto the silicon wafer, followed by exposure to UV light through a mask. Unexposed SU8 dissolves during development while the exposed SU8 remains onto the wafer as the desired pattern.

Before beginning the photolithography steps, the silicon wafer was placed in the oven for 10 minutes at 393 K. This was done to ensure that the moisture present on the surface of the silicon substrate was dried. Next followed spin-coating photoresist onto the substrate (Figure 3.4). For getting the pattern of nanochannels the layer of photoresist on spin coating must yield the thickness of 500 nm (as was

the desired depth of the nanochannels). SU8 2000.5 was the required photoresist that has a solid concentration of 14.3% [49]. However, due to unavailability of SU8 2000.5, dilution of a more viscous photoresist (SU8 2005) was performed. SU8 2005 has a solid concentration of 45%. Hence, SU8 2005 was diluted using the solvent cyclopentanone to obtain a solids concentration equivalent to that of SU8 2000.5. The diluted photoresist was poured over the silicon wafer and spin coated at a rate of 3000 rpm. The wafer coated with diluted photoresist was then soft baked at 368 K for 1 minute. During the process of soft baking, solvent on the top surface of the photoresist evaporates hardening the surface. Next followed the step of exposure of the photoresist to UV light for 6 seconds through the photomask using the contact exposure mode. The design of the mask is discussed in the preceding section. UV light passes through the transparent regions of the mask (the nanochannels) and falls onto the photoresist. SU8 is a negative photoresist consisting of highly branched epoxy derivative. Upon reaction with the UV light, small amount of strong acid is generated that opens up the epoxide rings of the resist and further catalyzes the cross linking reaction of the resist. The photoresist was then subjected to a post exposure bake at 368 K for 1.5 minutes during which the process of cross linking was further gets activated and completed. Next followed the step of development. A developer agent(1-methoxy-2-propyl acetate) was used to dissolve the unexposed parts of the resist while the fully polymerized SU8 (in the form of desired pattern of nanochannels) remained onto the wafer. Development was performed for 1 minute while making sure that the photoresist was completely immersed in developer chemical. It was also agitated to ensure fresh supply of the developer to the resist. The silicon wafer with the developed nanochannel pattern was then rinsed with Isopropyl Alcohol (IPA) for 10 seconds and air dried. A final hard bake was done at 423 K for 1.5 minutes that enhanced the hardness of the pattern.

It should be noted that during the patterning of nanochannels, the pattern of markers do not become visible after the post exposure baking step. The visibility of markers is important to proceed with the second photolithography step, in order to align the nanochannels with the microchannels. It was observed that only after developing the photoresist, the markers became visible. Hence, the entire sequence of steps till hard bake was followed for nanochannel patterning. This ensures that markers are visible for the second step of microchannel patterning while also making sure that the second development step of microchannels does not affect the already developed nanochannels.

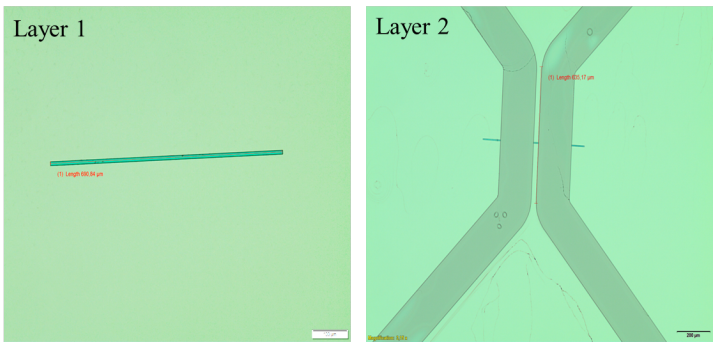


Figure 3.5: Photolithography involved patterning of the microchannels and nanochannels in two steps. Layer 1: Nanochannel obtained on the silicon wafer as a result of first step of photolithography. Layer 2: Microchannel aligned to the nanochannel, obtained after the second step of photolithography.

The patterning of nanochannels was followed by the patterning of microchannels following the same sequence of steps. SU8 2005 photoresist was used as such without dilution. The details of other steps have been summarized in Table 3.2.

After the fabrication of master (silicon wafer with the pattern of micro and nanochannels), it was important to characterize if the heights of the channels on the master were obtained as expected (500 nm for nanochannel and 5 $\mu$m for the microchannel). Profilometer was used to determine the heights of the channels(Figure 3.6). Channel profiles were obtained at various locations in the master and it was found that the heights of the channels were on an average 4.5 $\mu$m and 300 nm for the microchannel and nanochannel respectively. A sample height profile of the channels has been presented in Figure 3.6. Height profile at another location in the master can also be found in Appendix B.

Table 3.2: Summary of the experimental parameters used during photolithography step.

| | Specifications | |
|---|---|---|
| Processing Step | Nanochannel | Microchannel |
| Spin-coating speed | 3000 rpm (diluted SU8 2005) | 3000 rpm (SU8 2005) |
| Soft bake (at 368 K) | 1 minute | 2 minutes |
| Exposure time | 6 seconds | 10 seconds |
| Post exposure bake (at 368 K) | 1.5 minutes | 2.5 minutes |
| Development time | 1 minute | 1.5 minutes |
| Rinsing in IPA | 10 seconds | 15 seconds |
| Hard bake (at 423 K) | 1.5 minutes | 2 minutes |

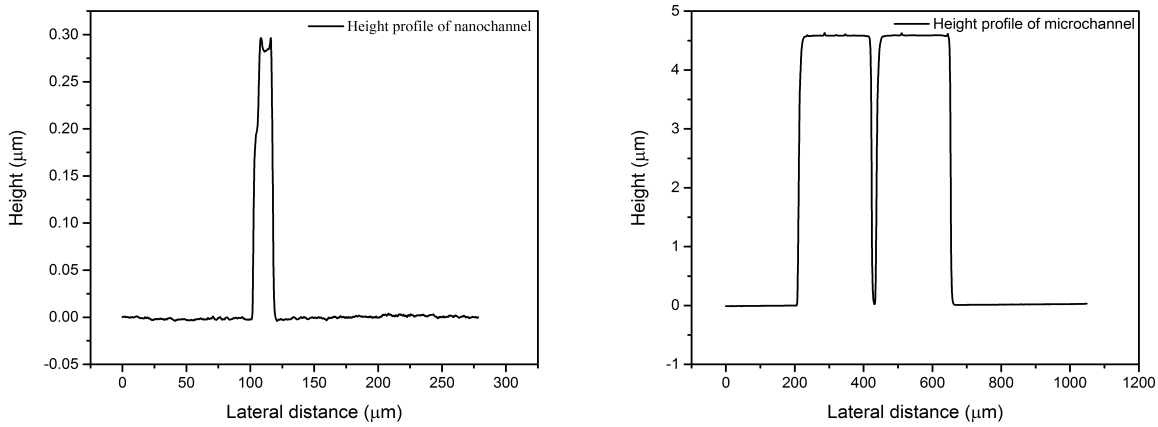


(a) (b)

Figure 3.6: The height of channels obtained on silicon wafer as a result of photolithography were characterized by profilometer.(a) Height profile of the nanochannel. The observed nanochannel height was 300 nm. (b) Height profile of the microchannel. The observed microchannel height was 4.5 $\mu$m.

### 3.2.3. Soft lithography

Photolithography performed in cleanroom leads to the fabrication of a master (silicon wafer with the microchannels and nanochannels). The master is then used as a mold to perform soft lithography, where a polydimethylsiloxane(PDMS) replica of the master is created [50].

The silicon wafer was first exposed to silanzing agent (1H,1H,2H,2H-perflurooctyl) in a vacuum chamber for ~3 hours. Coating the wafer with silanizing agent makes it hydrophobic and ensures that PDMS does not stick to it. The base and curing agent (Sylgard® 184) were then mixed in a ratio of 10:1. 70 g of base mixed with 7 g of curing agent was degassed to remove air bubbles. It was then poured over the silicon wafer in a petridish. A second degass step was performed to ensure there were no air bubbles between the wafer and PDMS. Following this, the wafer with PDMS was placed in the oven at 341 K for around 4 hours. The vinyl groups of base react with the silcion hydride groups present in curing agent and crosslink to yield to an elastomeric solid. The crosslinking is initiated by an organometallic reaction due to the presence of platinum based catalyst in the base[51]. The process is commonly referred to as hydrosilation of double bonds. An increased temperature only accelerates the cross linking reaction. Curing was followed by peeling off the PDMS elastomer and releasing it off the master. PDMS gets the negative imprint of the wafer and contains the pattern of channels in the form of valleys. The height profile of the channels obtained in the PDMS replica were the same as master (Appendix A). The PDMS was then cut out into blocks with each block containing a pattern of channels. It should be noted that the channels couldn't be seen on the PDMS because of the small depth of the channels. Pasting scotch tapes over the PDMS surface enabled to see the microchannels

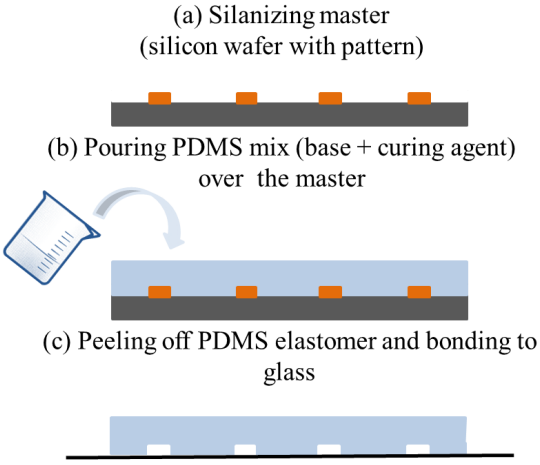


Figure 3.7: Schematic overview of soft lithography which allows to create a PDMS replica of the patterned silicon wafer.

which made it easy to cut out the PDMS. The holes for inlet and outlet of fluid were then made using bio-punches. This was followed by washing the blocks in absolute ethanol and drying to eliminate any dust particles or residual PDMS particles. The surface of the washed and dried PDMS blocks were then cleaned multiple times using scotch tape. A similar cleaning process was followed for glass slide (thickness #1). Thin glass slides were used due to imaging purpose (Section 3.3). The PDMS block and glass slide were then exposed to plasma for a duration of 2 minutes 20 seconds. The oxidized surfaces were then brought into contact quickly (<1 min) and pressed together to seal them. Pressing should be done carefully as a lot of force can cause the channels to collapse. Bonded devices (glass slide with PDMS) were kept in oven at 341 K for about 4 hours. The devices were then ready to use (Figure 3.8).

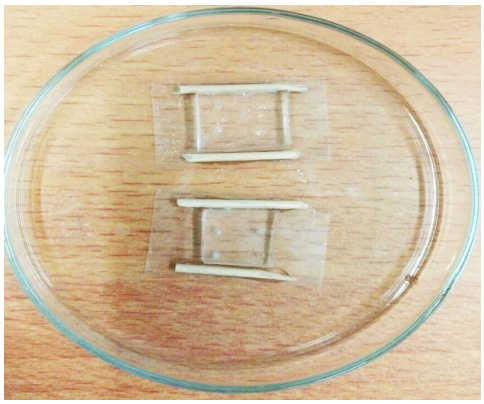

Figure 3.8: Hybrid nano/microfluidic device resulting after soft lithography. Sticks stuck to the thin glass slide on the sides keep the device firm and stable on microscope stage.

It was noticed that despite following the above procedure carefully, the nanochannels and microchannels were collapsing. This could be because of high aspect ratio (width/depth) of the channels and low Young's modulus of PDMS. Hence, two measures were taken to enhance the stiffness of PDMS to avoid channel collapse. The amount of curing agent was increased to 10 g (14.3 wt.%) and cured for an extended time (overnight). A combination of these steps seemed to solve the problem of channel collapse. The reason behind such an observation could be that the volatile smaller polymer chains and the unpolymerized prepolymer(that make PDMS soft) are driven off during extended curing periods [52]. Moreover, an optimal amount of 14.3 wt.% curing agent was also reported to increase the

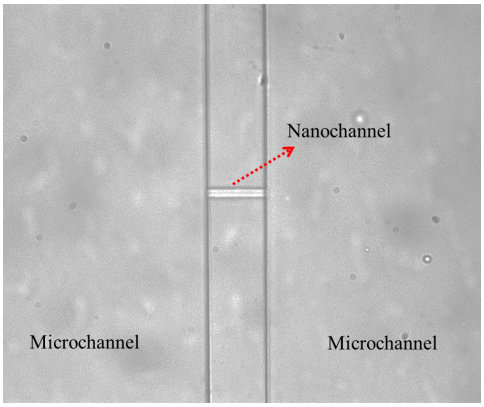


Figure 3.9: Microchannel and nanochannel as replicated in PDMS using soft lithography. Channels were imaged at 40X magnification.

mechanical strength [53].

## 3.3. Imaging using confocal microscope

The method proposed to find the diffusion coefficient of a particle in both microchannel and nanochannel was particle tracking. The particles chosen were 100 nm polystyrene beads and were suspended in glycerol/water mixture in order to visualize the particles in the channels. Particles in microchannel were tracked in 80/20 wt.% glycerol/water solution and particles in nanochannel were tracked in 30/70 wt.% glycerol/water solution with 1 mM KCl. Particles were visualized using confocal microscope. The following subsections describe sample preparation and visualization of particles in channels.

### 3.3.1. Sample preparation

To prepare 80/20 wt.% glycerol/demineralized water solution, 8 g of glycerol was mixed with 2 mL of demineralized water. Similarly 3 g of glycerol was mixed with 7 mL of demineralized water to prepare 30/70 wt.% glycerol/demineralized water solution. The mixture is ultrasonicated for about 30 minutes with vigorous shaking in between. The sample is then stored at room temperature in containers sealed with parafilm.

The preparation of 100 nm polystyrene nanobead solution, involved the dilution of the commercially available suspension of Fluospheres. One sample prepared was a nanobead solution in 80/20 wt.% glycerol/demineralized water mixture with a nanobead concentration of about $9\times10^5$ beads/mL. Another sample prepared was a nanobead solution in 30/70 wt.% glycerol/demineralized water mixture with a nanobead concentration of about $5\times10^9$ beads/mL. To calculate the number of beads/mL present in the commercially available suspension of Fluospheres, the following equation provided by the supplier was used [54]:

$$Microspheres/mL = \frac{6C10^{12}}{\rho\pi(2r)^3} \tag{3.1}$$

where $C$ is the concentration of suspended beads in g/mL provided by the supplier (0.02 g/mL), 2r is the diameter of the beads in $\mu$m and $\rho$ is the density of the polymer that makes the bead in g/mL (1.05 for polystyrene).

Dilution of the commercially available microsphere suspension was performed accordingly to obtain the aforementioned concentrations of beads in glycerol/demineralized water mixture. Potassium chloride salt (KCl) was also added to the nanobead solution in 30/70 wt.% glycerol/demineralized water such that the concentration of salt was 1 mM. Thereafter both the solutions of 80/20 and 30/70 wt.% were ultrasonicated for 30 minutes with vortexing in between. This was done to ensure that polystyrene beads were not sticking to each other and uniformly suspended in glycerol/water mixture.

### 3.3.2. Visualization of fluorescent beads in channels

In order to answer the research questions, particles were tracked in both microchannel and nanochannel using CLSM. The working principle of CLSM can be found in Appendix D. The excitation wavelength of the fluorescent particles was 580 nm and emission wavelength was 605 nm. Rhodamine filter was employed to be able to detect fluorescence. For the detection wavelength of 605 nm, the depth of focus is 683 nm(Equation D.2). For particle tracking in microchannel, the channels were filled with polsytrene suspension in 80/20 wt.% glycerol/demineralized water mixture. A viscous solvent was chosen for visualizing the Brownian motion of particles in the microchannel as it would prevent the particles from juggling in and out of the depth of focus and keep them in focus for a longer time. While for particle tracking in nanochannel, the channels were filled with polystyrene suspension in 30/70 wt.% glycerol/demineralized water mixture with 1mM KCl. The depth of focus was larger than the depth of nanochannel (300 nm). The entire channel was within the optical slice of good focus and particles were always in focus, which eliminated the use of viscous solvent. Moreover, nanochannel offered less resistance to the entry of less viscous solvent [55]. The presence of salt also helped overcome the problem of sticking of the beads to the nanochannel wall to a large extent.

Sample solution was first filtered using 0.2 $\mu$m filter to ensure it was free of dust particles. The channels were filled with sample solution using syringe pump. The tubings to the inlet and outlet ports were then withdrawn from the device and the ports were sealed using scotch tape. The device is left undisturbed for one hour before imaging. The device is then placed onto the sample stage of the confocal microscope. Imaging is done at room temperature (293$\pm$1 K) using oil immersion 40X objective (Zeiss, NA=1.3). An important point to be kept in mind is the working distance of the objective. Working distance(WD) is the distance between top lens of the objective and the sample at which the sample is in sharp focus [56]. WD of the used objective is 0.21 mm. Hence, #1 glass slide (thickness in the range of 0.13-0.16 mm) is used to seal PDMS (Figure 3.8). Laser power was kept at 20% of the maximum power. Images of size (512 pixels $\times$ 512 pixels) were recorded. A series of images (more than 50) were taken for each particle with a frame rate of 4 Hz. For each image scan time was 0.242 s with a pixel dwell of 0.39 $\mu$s. Hence, all pixels of a single image were scanned in a time of 0.102 s with the time between two images being 0.139 s ($\Delta$t). Pinhole size was kept at 1 $\mu$m. The other parameters used were gain: 720, digital offset: -50, digital gain: 0.7. It shall be noted that the observed motion of the particles in the channels was in the x and y plane.

## 3.4. Nanoparticle tracking

Following the image acquisition of particles in nanochannel and microchannel using confocal microscope, is the important step of nanoparticle tracking. This section describes how the images and data were analyzed, in order to answer the research questions.

### 3.4.1. Image analysis

The images acquired using confocal microscope, were bright fluorescent round particles on a dark background. Image analysis involved locating the position of particles in subsequent images. To do the same a Matlab code was used. The code followed the algorithm stated by Crocker and Grier which has been discussed below [57].

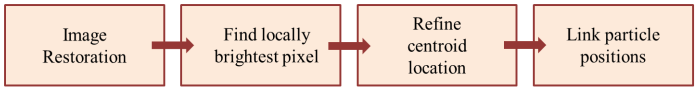


Figure 3.10: Schematic representation of step by step procedure followed to track particle positions using the tracker software.

The first step involves image restoration. The images might have imperfections in the form of noise and non-uniform contrast that make locating particle positions difficult. Variations in contrast are eliminated by using a boxcar average over a region greater than the particle size. A second filter (Gaussian

blurring) is performed on the same image to suppress noise [58].

In the second step the possible particle locations are identified as the locally brightest pixels. In order to find the particles, two input parameters have to be specified: the apparent size of the particle and threshold level. The size of the particles in the images acquired using confocal was found to be ~15 pixels. The threshold level allows to set a value on the scale of 1-255, which is an indication of the increasing level of brightness. The threshold level must be set such that the brightest pixels in a particle are identified. The threshold level was also set carefully such that only particles that were in focus were detected.

After the identification of brightest pixel in a particle, the centroid location is refined. In the method of identifying a single pixel at a position (x,y) of maximum brightness yields an accuracy of only about half a pixel. However, the algorithm provided by Crocker and Grier provides for refining the particle positions further to obtain an accuracy to better than 1/10 of a pixel. The local brightest pixel (x,y); is expected to be close to the actual geometric centre ($x_o$,$y_o$). The offset ($\epsilon_x$,$\epsilon_y$) between the two is found using the integrated brightness of the spherical particle. The location of centroid is then refined and returned as (x+$\epsilon_x$,y+$\epsilon_x$).

In a similar way, for every frame, the particle locations are identified. However, the next important step is to link the particle positions from frame to frame, in order to get its trajectory. This requires the user to input the third parameter of maximum displacement. This parameter is an estimate of the maximum distance the particle moves in a single time interval [58]. Hence, it should be ensured that only a few particles are present in each frame with sufficient distance from each other. To avoid any confusion of mixing up tracks of two different particles, it is wise to watch the video from beginning till end ensuring enough inter particle separation is maintained.

### 3.4.2. Data analysis

Image analysis returns an output of particle locations in every frame. These locations can be linked together to find the particle trajectory, as depicted in Figure 3.11.

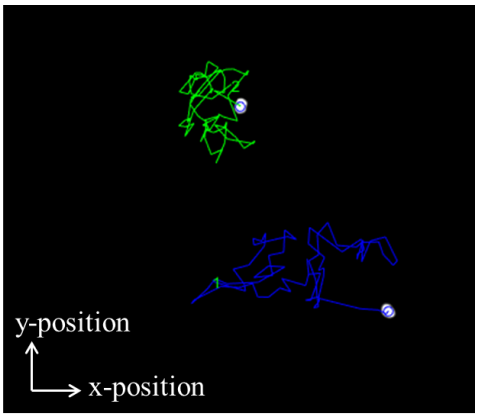


Figure 3.11: Particle trajectory (green and blue thread) of two different particles (white circles) as obtained from image analysis.

The obtained positions for particle ($x_i$, $y_i$) in every frame is a position after a time step of Δt (Section 3.3.2). Hence, for every Δt, the displacement of the particle can be found as [59]:

$$\begin{aligned} \Delta x_i &= x_{i+1} - x_i \\ \Delta y_i &= y_{i+1} - y_i \end{aligned} \tag{3.2}$$

As already discussed in Section 2.1.2, the diffusion coefficients are related to microscopic step lengths of Δx and Δy and the time gap between two steps. Moreover, the probability distribution of a

particle following random Brownian motion forms a bell shaped curve. Hence, after the obtaining the particle displacements for a particle, the histogram of displacements is plotted. A Gaussian curve is then fit to the frequency distribution of both the x and y displacements using the equation [60]:

$$P(x) = \frac{1}{\sigma_x\sqrt{2\pi}} e^{-\frac{(\Delta x - \langle \Delta x \rangle)^2}{2{\sigma_x}^2}}$$
$$P(y) = \frac{1}{\sigma_y\sqrt{2\pi}} e^{-\frac{(\Delta y - \langle \Delta y \rangle)^2}{2{\sigma_y}^2}} \quad (3.3)$$

$\sigma^2$ is the variance from Gaussian fit to the 1D x and y displacements. The relation between one dimensional mean squared displacement, $\langle \Delta x^2 \rangle$ and variance is given by [61]:

$${\sigma_x}^2 = \langle \Delta x^2 \rangle - \langle \Delta x \rangle^2 \quad (3.4)$$

When the mean, $\langle \Delta x \rangle$ is zero, the variance from Gaussian fit to the displacement histogram becomes equal to the mean squared displacement, which is then used to estimate the one dimensional diffusion coefficients as:

$${\sigma_x}^2 = \langle \Delta x^2 \rangle = 2D_x \Delta t$$
$${\sigma_y}^2 = \langle \Delta y^2 \rangle = 2D_y \Delta t \quad (3.5)$$

In order to find the mean diffusion coefficients, arithmetic average of $D_x$ and $D_y$ can be taken. Another alternative is to combine the displacements, plot a frequency distribution, perform a Gaussian fit and obtain the diffusion coefficient in the same way as described above. All gaussian fittings were performed using Matlab inbuilt function normfit.

# 4

# Results and Discussion

In this chapter, the results obtained during the research have been presented. A thorough discussion of the results has also been provided while attempting to answer the research questions. To begin with, Section 4.1 presents the results and discussion pertaining to the reliability of the experimental method. A preliminary analysis was carried out to confirm the soundness of image and data analysis method. Section 4.2 discusses results of particle tracking of 100 nm polystyrene beads in microchannel in 80/20 wt.% glycerol/demineralized water mixture. An estimate of the expected value of diffusion coefficient was first made taking into account variable sources of uncertainty. The experimentally obtained diffusion coefficient is presented, compared to expected results and its statistical significance is discussed. Finally, follows a discussion on how the results of particle tracking in microchannel can be extrapolated for comparison with tracking results in nanochannel. Section 4.3 discusses in detail results of particle tracking of 100 nm polystyrene beads in nanochannel in 30/70 wt.% glycerol/demineralized water mixture with 1 mM KCl. The analysis is split into parts, based on the observed value of diffusion coefficients. For the first part of analysis the diffusion coefficients of the 100 nm beads in 300 nm high nanochannels are presented and compared to the diffusion coefficients in bulk systems (obtained from particle tracking in microchannel). The deviation of observed diffusion coefficients from bulk value is analyzed through different lenses: hydrodynamic interactions, double layer formation, Van der Waals forces and increased viscosity.

## 4.1. Reliable estimate of diffusion coefficient

In order to draw reliable conclusions, it was important to ensure that the experimental method of determining diffusion coefficients was reliable. Hence, the results of the preliminary tests carried out to establish the reliability of the image and data analysis method have been presented and discussed. Section 4.1.1 discusses in detail the accuracy with which the particle locations were found using the tracker software. On the other hand, Section 4.1.2 discusses about the minimum number of displacements (or data points) that were considered for each particle to draw reliable estimates of diffusion coefficients.

### 4.1.1. Sensitivity study of the image analysis technique

The diffusion coefficients in the project were measured by the method of particle tracking. The tracker software that has been employed follows the algorithm given by Crocker and Grier and has been discussed in Section 3.4[57]. The input parameters that were provided to the tracker to obtain the particle centroid positions were particle diameter in pixels and threshold level (on a scale of 1 to 255). A preliminary study was carried out to understand the accuracy of centroid location and how the input of the aforementioned parameters (particle size and threshold level) affect the output of coordinates of the centroid.

Locating particles with accuracy is of paramount importance to make reliable conclusions about diffusion coefficient. The software first locates possible particle positions by identifying local brightness

maxima. A pixel is identified as possible particle position if there are no brighter pixels in a region *w* around it, where *w* is an integer larger than the apparent particle radius. In this method of identifying a single pixel at a position (x,y) of maximum brightness yields an accuracy of only about half a pixel. However, the algorithm provided by Crocker and Grier provides for refining the particle positions further to obtain an accuracy to better than 1/10 of a pixel. The local brightest pixel (x,y); is expected to be close to the actual geometric centre ($x_o$,$y_o$). The offset ($\epsilon_x$,$\epsilon_y$) between the two is found using the integrated brightness of the spherical particle. The location of centroid is then refined and returned as (x+$\epsilon_x$,y+$\epsilon_x$). In order to verify this claim by the algorithm of the tracker software, a white spherical particle of diameter 15 pixels was drawn on a black canvas using ImageJ (image on the left in Figure 4.1). The image of particle was blurred using the smooth tool of ImageJ. This inbuilt smooth function of ImageJ, replaces each pixel with an average value in a neighbourhood of size 3×3 . Furthermore, Gaussian noise (of standard deviation 2) was added to it. The coordinates of centre of this particle was known and was used an input image for the tracker software. The tracker software was then asked to locate the centre of the particle. The coordinates of centre returned by the software was compared to the actual known centre coordinates of the particle. The results of the analysis are tabulated and presented in Table 4.1.

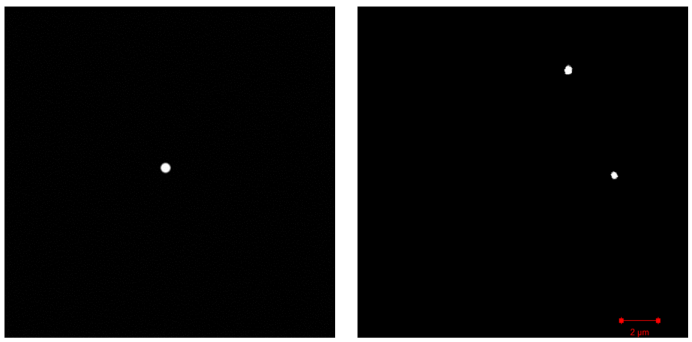

Figure 4.1: Left: Artificial image created on ImageJ. Right: Sample image taken from confocal laser scanning microscope.

It can be seen that when the size input to the tracker software was 15 pixels, which was the actual apparent size of the bead, the centroid of the particle was located with accuracy to better than 1/10 of a pixel. When the size input to the tracker software was smaller than actual apparent size of the bead, the accuracy with which the centroid was located decreases. Moreover, for a size of 8 pixels the deviation from the actual centre position was found to be quite large. It was found that the window of $8times8$ pixels was not centered around the particle, but shifted towards the edge. When the input to the tracker software was a size greater than the actual size of 15 pixels, the accuracy was not altered. A greater size simply increases the run time of the software as now the tracker explores a larger area. Hence, for analyzing the images obtained from the confocal microscope, the apparent size of the bead was always first measured on ImageJ and the input to the tracker was a size 2-3 pixels greater than the measured value, to ensure accurate location of centroid.

Table 4.1: Result of accuracy test of the tracker software. $\epsilon_x$ and $\epsilon_y$ is the offset/difference between the actual centre position of the image and the centre position returned by the software.

| Particle size input (pixels) | $\epsilon_x$ (pixel) | $\epsilon_y$ (pixel) |
|---|---|---|
| 8 | 1.18 | 2.77 |
| 10 | 0.39 | 0.38 |
| 12 | 0.26 | 0.24 |
| 15 | 0.02 | 0.01 |
| 17 | 0.02 | 0.01 |
| 20 | 0.02 | 0.01 |

A sensitivity study for the input of threshold level to the tracker was also conducted to understand

if the input of threshold level affected the centre position returned by the software. The threshold level in the software allowed to set a value on the scale of 1-255, which is an indication of the brightness of pixel in the image. This input of threshold was varied for an image taken from confocal microscope and it was observed if the coordinates of centre returned by the software were affected or not. An image taken from the confocal microscope using settings mentioned in the experimental section and with a particle of size ~15 pixels (image on the right in Figure 4.1) was used for checking the sensitivity to threshold level. The option of threshold allowed to fix a minimum brightness level only beyond which the particle would be detected. The input threshold level was varied and kept at 30%, 40%, 50%, 70% and 80% of the maximum detectable level.

Table 4.2: Result of threshold sensitivity test of the tracker software. *x,y* are the centroid location returned by the software. The centroid location corresponds to the position of one of the particles in the image on the right in Figure 4.1

| Threshold level (as a % of the maximum detectable threshold level) | *x* (pixel) | *y* (pixel) |
|---|---|---|
| 30 % | 326.99 | 99.04 |
| 40% | 326.99 | 99.04 |
| 50 % | 326.99 | 99.04 |
| 70 % | 326.99 | 99.04 |
| 80 % | 326.99 | 99.04 |

It was found that the *x* and *y* positions returned as the centre of the particle was not affected by changing the threshold level (Table 4.2). This was possibly due to the settings used for capturing images using confocal microscope. A negative value of digital offset was used, which enhances the contrast: makes the darker regions darker and uses the entire range of brightness [62]. Thus, by reducing the background level, it performs a processing step already during the time of image acquisition using full range of brightness. The dark regions in the background of the image are at 0 value while the position corresponding to the particles have bright pixels . Hence, for analyzing images, threshold level was freely chosen in such a way that the out of focus particles were rejected and only desired particles were tracked.

Hence, it was concluded that tracker software returned centroid positions of the particles with accuracy to better than 1/10 of a pixel when the apparent size of particle was input correctly. Moreover, the image acquisition settings ensured that centroid location was not sensitive to the input of threshold level.

### 4.1.2. Optimization of the data processing method

Once the reliability of the tracking method was confirmed, it was also pertinent to establish the reliability of the data analysis method. It was important to determine the minimum number of displacements/frames per particle in order to obtain a reliable estimate of diffusion coefficient. To understand the same, it is first explained how a typical measurement of diffusion coefficient for a single particle was done. Thereafter, a small discussion is presented on the optimum number of frames for an individual particle and combining the displacements of multiple particles.

Using the tracker software, particle positions in every frame were found in order to determine frame to frame displacement. Once the frame to frame displacements were obtained, a histogram of these displacements were created. This was followed by fitting a Gaussian curve over the obtained frequency distribution. Figure 4.2a and 4.2b represent the histogram of 40 x and y displacements of a single particle with Gaussian fit performed over it. The variance from the Gaussian fit results in the 1D diffusion coefficients, $D_{x,micro}$ and $D_{y,micro}$, using the relation (Section 3.4.2):

$$\begin{aligned} \langle \Delta x^2 \rangle &= 2D_x \Delta t \\ \langle \Delta y^2 \rangle &= 2D_y \Delta t \end{aligned} \tag{4.1}$$

$\langle \Delta x^2 \rangle$ and $\langle \Delta y^2 \rangle$ is equivalent to the variance of the fit performed while $\Delta t$ is the time between displacements (Section 3.3). In order to obtain the average diffusion coefficient, a histogram of the

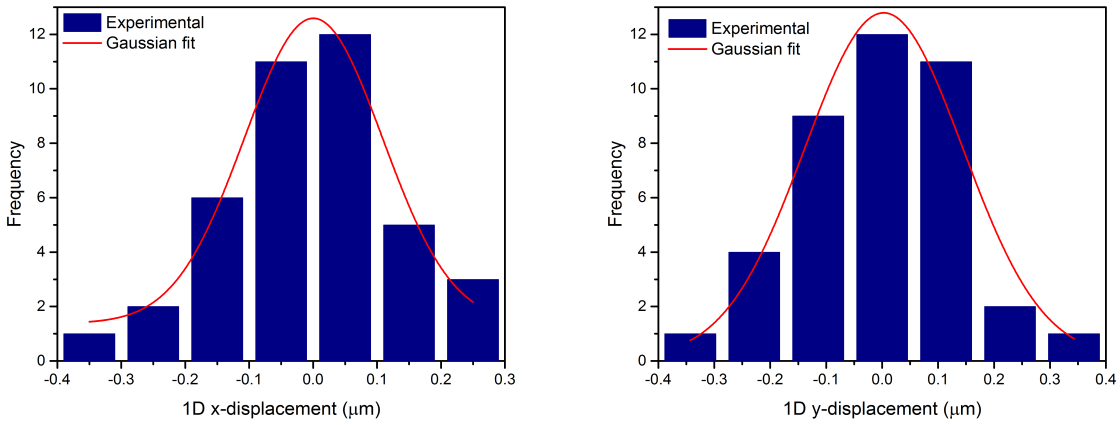


(a) (b)

Figure 4.2: Gaussian fit performed to the frequency distribution of 40 (a) x-displacements and (b) y-displacements of a single particle in the microchannel.

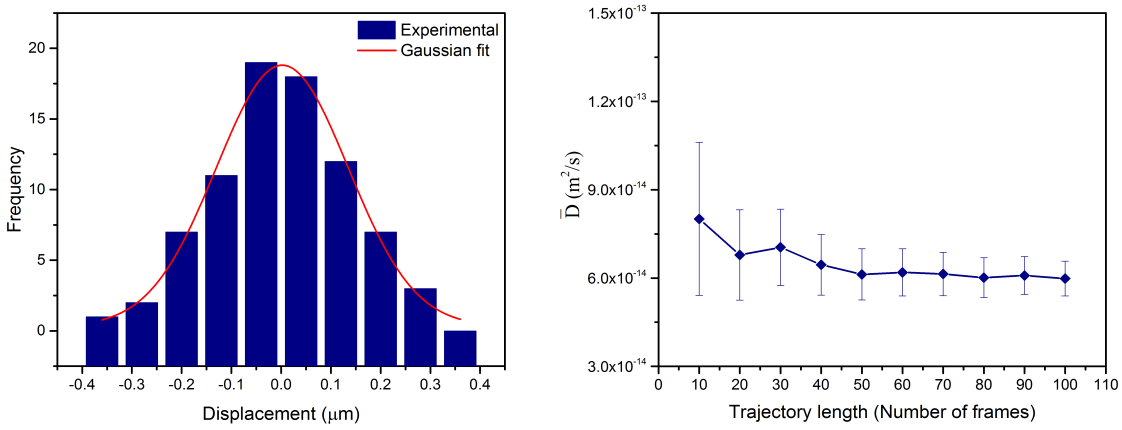


(a) (b)

Figure 4.3: (a) Gaussian fit performed to the combined x-displacements and y-displacements of a single particle in the microchannel to obtain the average diffusion coefficient. The trajectory length of the particle was 40. The individual x and y displacement histograms have been presented in Figure 4.2. (b) Average value of diffusion coefficient obtained for a single particle in microchannel as a function of number of frames. The error bars represent the sampling error.

combined x and y displacement was created. Gaussian fitting was performed over the distribution (Figure 4.3a) and the variance from the fit was used to obtain the average diffusion coefficient. Figure 4.3b represents the average value of diffusion coefficient as a function of the number of frames, obtained for a single particle. In order to obtain the average diffusion coefficient corresponding to the different number of frames, the same method was followed as described above for a particle with 40 displacements. It was observed from Figure 4.3b, that for a single particle the obtained value of the average diffusion coefficient displayed a stabilizing trend for a trajectory length greater than 50. Moreover, the uncertainty in the average value of diffusion coefficient (represented by the error bars in Figure 4.3b) also became the least and alike. This uncertainty is known as the sampling error. It is the standard error in the variance of the normally distributed displacements [63]. The fractional sampling

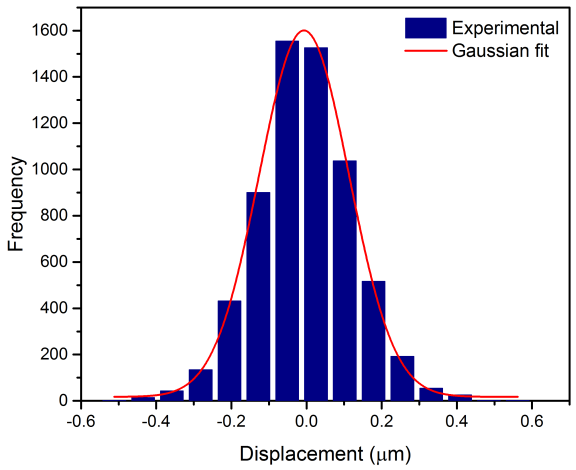


Figure 4.4: Gaussian fit performed to the combined x-displacements and y-displacements of 10 particles in the microchannel. The trajectory length for each particle was more than 50.

error is estimated by:

$$\sigma_{sampling} = \sqrt{\frac{2}{n-1}} \tag{4.2}$$

where n is the number of samples in the frequency distribution. The discussion till now was restricted to a single particle. What would happen if the displacements of multiple particles are combined together? In order to understand the same, Figure 4.4 further represents the combined x and y displacement histogram of 10 particles. The trajectory length of each individual particle was maintained more than 50, owing to the observation made in Figure 4.3b. The benefit of combining the displacements of multiple particles together is that the number of samples in the histogram increases, leading to a more smooth and regular histogram. The distribution and curve fitting gets better and approaches a limiting distribution [64]. Moreover, the increased number of samples in the frequency distribution also lead to a smaller sampling error. For instance, the average diffusion coefficient obtained from a single particle with a trajectory length of 100 (Figure 4.3b) was $5.88\times10^{-14}$ $m^2/s$ with an uncertainty of $\pm0.59$. On the other hand, the combined displacement histogram of 10 particles in Figure 4.4 (with each particle having a trajectory length of more than 50), resulted in an average diffusion coefficient of $5.89\times10^{-14}$ $m^2/s$ with an uncertainty of $\pm0.21$.

Hence, on the basis of observed trends, it was concluded that a minimum of 50 frames was required for each particle. Moreover, to draw reliable estimates of diffusion coefficients from particle tracking in the microchannel and nanochannel, a number of particles were tracked and their displacements combined.

## 4.2. Diffusion coefficient in microchannel

As already mentioned previously, investigation of diffusion of an analyte in the same device exhibiting different behavior in the microchannel and nanochannel is important. This would aid in drawing reliable conclusions. In this section, results and discussion pertaining to diffusion coefficients found in the microchannel have been presented. Section 4.2.1 summarizes the theoretical estimate of diffusion coefficient in microchannel taking into account sources of uncertainty. Section 4.2.2 summarizes the experimental result of diffusion coefficient in microchannel while also comparing it to the theoretical estimate found in Section 4.2.1. Finally, follows a discussion in Section 4.2.3, on how the results of particle tracking in microchannel were extrapolated for comparison with tracking results in nanochannel.

### 4.2.1. Expected value of diffusion coefficient in microchannel

Diffusion of particles in microchannel will follow diffusion behaviour as expected in free/unbounded solution. Hence, an estimate of the expected value of diffusion coefficient ($D_{bulk}$)in the microchannel from particle tracking experiments was made using the Stokes Einstein equation (Equation 2.8):

$$D_{bulk} = \frac{k_B T}{3\pi\eta D_h} \tag{4.3}$$

The variables in the aforementioned equation are temperature (T), viscosity of solvent ($\eta$) and hydrodynamic diameter of the solute ($D_h$). In estimating the values of these variables and hence the diffusion coefficient, the inevitable occurrence of uncertainties were also accounted for.

Sample used for particle tracking in the microchannel was 100 nm polystyrene beads suspended in 80/20 wt% glycerol/demineralized water, the preparation of which has been described in Section 3.3. All measurements were performed at room temperature (T) of 293 K. However, temperature fluctuations were unavoidable and an uncertainty of 1 K was included while evaluating $D_{bulk}$.The hydrodynamic diameter($D_h$) of polystyrene beads suspended in 80/20 wt% glycerol/demineralized water was estimated using Dynamic Light Scattering. It was found to be 120 nm with an uncertainty of 1 nm ($\delta D_h$) [65]. Viscosity ($\eta$) of the solvent is temperature dependent. To evaluate the viscosity of glycerol/water mixture at a specific temperature, the empirical formula proposed by Nian Shen Cheng (2008) was used[66]. The reason why viscosity-temperature correlations proposed in the study by Cheng were employed to predict $\eta$ is that these formulations were matched with three other databases and were found to be in good agreement (average error remained less than 2%) [67–69]. The formulation proposed is as mentioned below:

$$\eta = \eta_w^{\alpha}\eta_g^{1-\alpha} \tag{4.4}$$

where, $\eta_w$ is dynamic viscosity of water and $\eta_g$ is dynamic viscosity of glycerol. They are in turn dependent on T. $\alpha$ is further a function of other variables($C_m$) and coefficients (*a, b).* $C_m$ is mass percentage of glycerol in the range of 0-100 % while *a* and *b* are T dependent coefficients. The equations are valid in the T range of 273-373 K. The relations are as mentioned below:

$$\begin{aligned} \alpha &= 1 - C_m + \frac{abC_m(1-C_m)}{aC_m + b(1-C_m)} \\ a &= 0.705 - 0.0017T \\ b &= (4.9 + 0.036T)a^{2.5} \\ \eta_w &= 1.790exp\frac{(-1230-T)T}{36100+360T} \\ \eta_g &= 12100exp\frac{(-1233+T)T}{9900+70T} \end{aligned} \tag{4.5}$$

Using Equations 4.4 and 4.5, $\eta$ of 80/20 wt% glycerol/demineralized water ($C_m$ = 80) at T = 293 K was estimated to be 59.5 cP. It shall be noted that temperature fluctuations of 1 K would also cause fluctuations in the value of $\eta$ obtained for the solvent. Hence, uncertainty in the value of 59.5 cP caused by a change of T by 1 K is estimated. Uncertainty in viscosity ($\eta$), which is a function of temperature (T), was obtained by using method of error prorogation [64]:

$$\delta\eta = \frac{d\eta}{dT}\delta T \tag{4.6}$$

where $\delta\eta$ is the uncertainty in viscosity, $\delta$T is the uncertainty in temperature.

To obtain $\delta\eta$, the derivative of $\eta$ with respect to T was obtained using inbuilt Matlab function diff and then evaluated at 293 K using vps and subs function of Matlab. The uncertainty in viscosity for temperature fluctuations of 1 K was found to be 3.8 cP.

After obtaining the values of variables and uncertainties of individual variables, the expected value of $D_{bulk}$ was found using Equation 2.8. The uncertainty in $D_{bulk}$ ($\delta D_{bulk}$) was estimated using method of error propagation[64]:

$$\frac{\delta D_{bulk}}{D_{bulk}} = \sqrt{\left(\frac{\delta T}{T}\right)^2 + \left(\frac{\delta \eta}{\eta}\right)^2 + \left(\frac{\delta D_h}{D_h}\right)^2} \tag{4.7}$$

Hence, the expected value of diffusion coefficient from particle tracking in the microchannel was $(6.01 \pm 0.39) \times 10^{-14}$ $m^2/s$. This theoretical estimate was used for comparison with the experimental results in the following section, to conclude if the results found experimentally agreed well with what was expected.

### 4.2.2. Experimental estimate of diffusion coefficient in microchannel

This section summarizes the result of diffusion coefficient found by particle tracking in microchannel. A comparison is drawn between the experimental and theoretical results and a short discussion on the sources of errors has been presented.

Sample used for particle tracking in the microchannel was 100 nm polystyrene beads suspended in 80/20 wt% glycerol/demineralized water. 45 particles with a total of 6533 x and y-displacements each were analyzed to yield the experimental diffusion coefficient. Particles were tracked using the software described in Section 3.4. Once the frame to frame displacements were obtained, a histogram of these displacements were created. Gaussian fit over the obtained frequency distribution was performed to obtain the 1D diffusion coefficients (Section 3.4.2):

$$\begin{aligned} \langle \Delta x^2 \rangle &= 2D_x \Delta t \\ \langle \Delta y^2 \rangle &= 2D_y \Delta t \end{aligned} \tag{4.8}$$

Figure 4.5 represents the histogram of 6533 x and y displacements each with Gaussian fit performed over it. The mean from the Gaussian fit to the x and y displacement histogram was found to be 1.5 nm and 5 nm respectively. For a displacement of 5 nm, the contribution by velocity/drift is 1000 times less than that by diffusion[70]. It will be even smaller for a displacement of 1.5 nm. Hence, it can be concluded that convection was absent from the experiments.

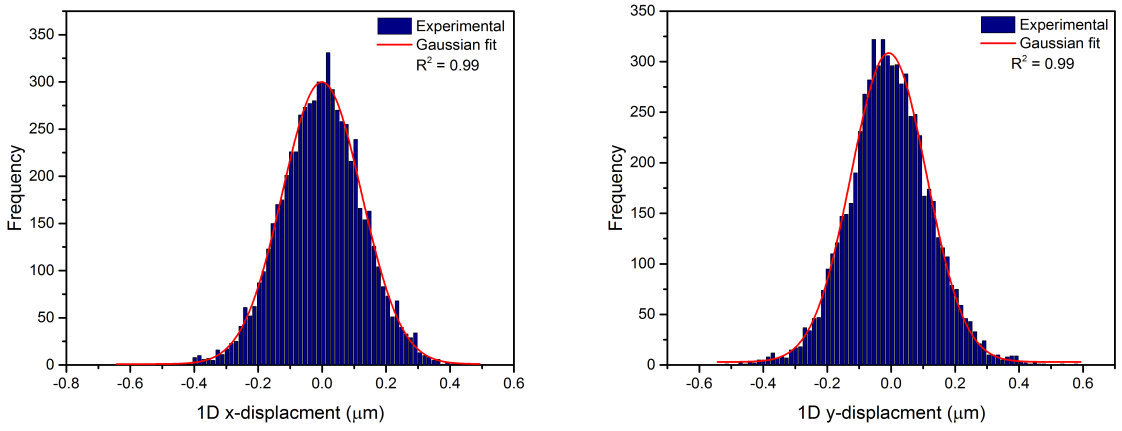


(a) (b)

Figure 4.5: Gaussian fit performed to the frequency distribution of the 6533 (a) x-displacements and (b) y-displacements in the microchannel. The variance from Gaussian fit to x-displacement histogram is 0.0161 $\mu m^2$ and the variance from Gaussian fit to y-displacement histogram is 0.0163 $\mu m^2$.

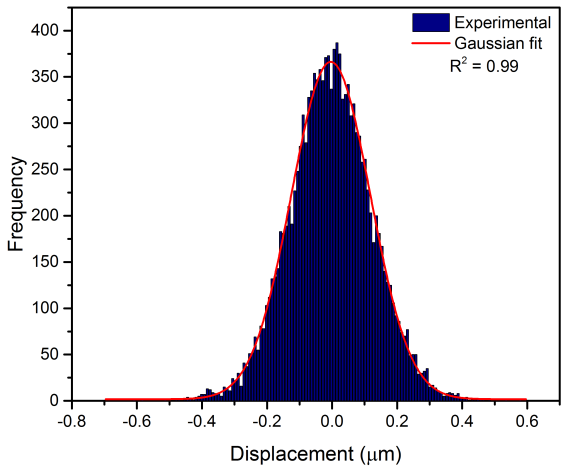


Figure 4.6: Gaussian fit performed to the combined x-displacements and y-displacements in the microchannel. The variance from Gaussian fit to total displacement histogram is 0.0162 $\mu m^2$.

Equation 4.8 can be used to estimate $D_{x,micro}$ and $D_{y,micro}$. $\langle \Delta x^2 \rangle$ and $\langle \Delta y^2 \rangle$ is equivalent to the variance of the fit performed. $\Delta t$, the time between displacements, is 0.139 s (Section 3.3). To obtain the average diffusion coefficient ($D_{micro}$), a histogram of both the x and y displacement was created, Gaussian fitting was performed over the distribution (Figure 4.6) and the variance from the fit was used. The values of diffusion coefficient obtained from the experiments are presented and a comparison with the expected value is drawn (Table 4.3).

Table 4.3: Summary of the experimental and expected values of diffusion coefficient as obtained in the microchannel

| Expected result ($10^{-14}$ $m^2/s$) | Experimental result ($10^{-14}$ $m^2/s$) | Relative difference | t-statistic |
|---|---|---|---|
| $D_{bulk}$ = 6.01±0.39 | $D_{x,micro}$ = 5.79±0.10 | 3.7% | 0.55 |
| | $D_{y,micro}$ = 5.88±0.10 | 2.2% | 0.32 |
| | $D_{micro}$ = 5.84±0.07 | 2.8% | 0.43 |

The uncertainty of ±0.1 in the experimental results is known as the sampling error. It is the standard error in the variance of the normally distributed displacements [63]. The fractional sampling error is given by:

$$\sigma_{sampling} = \sqrt{\frac{2}{n-1}} \tag{4.9}$$

where n is the number of samples in the frequency distribution.

The number of displacements collected for particle tracking in the microchannel are n = 6533(for each of the x and y displacements). This results in an error of 1.8%. $\sigma_{sampling}$ accounts for the uncertainty of the experimental results. It should be noted that even though $\sigma_{sampling}$ is 1.8%, relative difference with the nominal expected value of diffusion coefficient ($D_{bulk}$) is greater than 1.8% (Table 4.3). This disagreement is attributed to other sources of error. It has been reported in a finding that errors in Brownian motion experiments come from several random sources: temperature fluctuations, tracking error, drift, vibration and uncertainty in bead radius [61]. Drift/convection was absent in our experiments as already mentioned before. Moreover, the subpixel accuracy of the centroid locating algorithm has been demonstrated in Section 4.1.1. The 100 nm polystyrene beads used in the experiments had a coefficient of variation of 5%, as specified by the supplier [54]. These particles are

quite mono disperse and are not expected to have a significant effect on the value of $D_{micro}$. This has also been shown by Catipovic et.al.(2013) wherein beads used had a coefficient of variation of ~8%. Computational and experimental determinations revealed that bead size variation resulted in uncertainties that could be ignored. Error due to vibration was also simulated. Random values to the x and y displacements with a standard deviation of 50 nm was added and the resulting error was found to be around 3%. Furthermore, temperature changes were concluded to not play a significant role in increasing experimental uncertainty. However, in their study particles were tracked in water for which viscosity uncertainty due to temperature fluctuations were only around 2%. Temperature fluctuations in this study can create an uncertainty of 6.4% in viscosity, as estimated in Section 4.2.1. Hence, based on the aforementioned findings, observed relative error of about ~3% between $D_{bulk}$ and $D_{micro}$ can be attributed to vibrational noise and temperature fluctuations.

Next question that arises is about the statistical significance and closeness of the experimental result to the expected result. This is depicted by the value of t-statistic in Table 4.3. t-statistic is estimated as [71]:

$$t = \frac{D_{bulk} - D_{micro}}{\sqrt{\delta D_{bulk}{}^2 + \delta D_{micro}{}^2}} \tag{4.10}$$

The t value is an indication of number of standard deviations separating the two mean values. When the value of t is less than 1, it is reasonable to conclude that the two values being compared agree with each other. When t>2, the closeness of two values is questionable. In that case the probability of the two values being equal is below 5%. The highest t-statistic value found in the experiments for tracking in microchannel is 0.55 (Table 4.3). This implies a discrepancy of 0.55 standard deviations. The fractional area beyond $0.55\sigma$ is ~60%, as observed from Gaussian distribution tables [72]. This indicates that 6 out of 10 experiments would yield the result as reported in this study.

Hence, on the basis of comparisons drawn, it was concluded that the experimental results of particle tracking in microchannel were consistent with theoretical estimate and statistically significant.

### 4.2.3. Using diffusion coefficient obtained in microchannel

In the preceding sections, the agreement of experimental results of particle tracking in microchannel to the expected results reveal that the method of determining diffusion coefficient was reliable. This section further discusses how the results from particle tracking in microchannel was used to compare particle tracking results in nanochannel.

The solvent used to track particles in the microchannel was 80/20 wt% glycerol/water mixture. The reason behind using a viscous system stems from the fact that viscous solvent slows down the random Brownian motion of the polystyrene beads. This ensures that particles remain in focus for a longer time and served the purpose of particle tracking in microchannel. However, the same solvent could not be used to track particles in the nanochannel. Firstly, for the viscosity of 80/20 wt% glycerol/water mixture, the hydraulic resistance offered per unit length by the 5 $\mu$m wide and 300 nm high nanochannel to fluid flow is approximately $2\times10^5$ times higher than that offered by the microchannel (200 $\mu$m wide and 4.5 $\mu$m high) [55]. This was combined with the problem of using distilled water alone as a solvent as the channels were made out in PDMS. The surface of PDMS is hydrophobic and water does not wet the surface easily [73]. As mentioned in Section 3.3, the solvent that catered to the requirement of particle tracking in the nanochannel is 30/70 wt% glycerol/water mixture with KCl salt concentration of 1 mM. Hence, for comparison with the particle tracking results in the nanochannel, a value of diffusion coefficient that would be observed in the same solvent in an unconfined system is required. For this purpose, the experimental result, $D_{micro}$, of particle tracking in microchannel was used.

Diffusion coefficient is proportional to $1/(\eta D_h)$. Hence, the diffusion coefficient of 100 nm polystyrene beads in 30/70 wt% glycerol/water mixture with 1 mM KCl ($D_{unconfined}$) can be given by:

$$D_{unconfined} = D_{micro} \times \frac{\eta_{80/20} D_{h,80/20}}{\eta_{30/70} D_{h,30/70}} \tag{4.11}$$

where $\eta_{80/20}$ , $D_{h,80/20}$ and $\eta_{30/70}$ , $D_{h,30/70}$ are viscosity and hydrodynamic diameter of 100 nm polytsyrene beads in 80/20 wt% glycerol/water and 30/70 wt% glycerol/water mixture respectively.

$\eta_{30/70}$ was estimated following the method as described in Section 4.2.1. It was found to be 2.35 cP. Temperature fluctuations of 1 K introduce an uncertainty of $\pm$0.07 in $\eta_{30/70}$. Concentration of KCl is too low to affect the viscosity of solvent [74, 75]. $D_{h,30/70}$ on the other hand, is estimated to be (124$\pm$2) nm using Dynamic Light Scattering [65]. A larger hydrodynamic diameter is expected in 30/70 wt% glycerol/water mixture due to the presence of salt.

Hence, using Equation 4.11 and applying the rules of error propagation [64], the diffusion coefficient of 100 nm polystyrene beads in 30/70 wt% glycerol/water mixture was found to be (14.31$\pm$1.04)$\times 10^{-13}$ $m^2/s$. This was indeed the diffusion coefficient that would result from particle tracking experiments in a solvent medium of 30/70 wt% glycerol/water and in the absence of confinement effects. Particles were tracked in the same medium in the nanochannel and were compared to the value of (14.31$\pm$1.04)$\times 10^{-13}$ $m^2/s$ ($D_{unconfined}$) in order to make reliable conclusions on confinement effect. This method of comparison makes the result more rational as a comparison is drawn between diffusion coefficients measured in the same experimental manner, in the same device.

## 4.3. Diffusion coefficient in nanochannel

In this section, the results and discussion pertaining to particle tracking in nanochannel have been presented. Firstly, it is explained in Section 4.3.1 why the analysis of results in nanochannel was split into parts, to be in line with the research questions. Furthermore, in Sections 4.3.2 and 4.3.3 the extent of deviation of results from bulk systems is quantified and the possible reasons for the deviation have been discussed.

### 4.3.1. Division of analysis into two parts

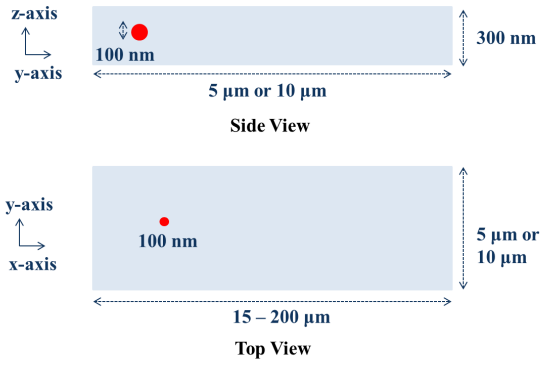


Figure 4.7: Side view and top view of nanochannels.

100 nm polystyrene beads were tracked in nanochannels. The top and side view of the nanochannel has been presented in Figure 4.7. The depth of nanochannels was 3 times the diameter of the particle. The presence of a wall at a finite distance from the particle in the z-direction, was expected to produce interesting results. The observed motion of the particle was in the xy plane as explained in Section 3.4.

However, analysis of particle tracking in nanochannel was found to return two kinds of output. The diffusion coefficients of individual particles in the nanochannel ($D_{nano}$) was spread over a wide range of values. $D_{nano}$ fell into two distinct ranges. To understand the manifestation of two extreme values

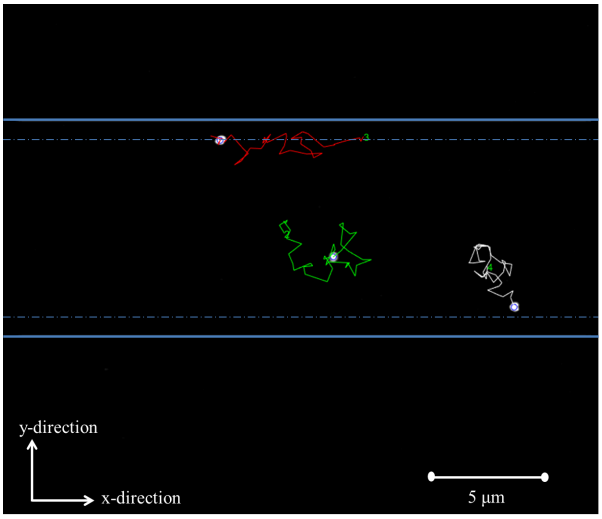


Figure 4.8: Tracks followed by particles inside the nanochannel (red, green and white colour). Solid blue line is the boundary of 10 $\mu$m wide nanochannel (y-direction). Dashed blue line encloses a region of 1 $\mu$m from the side walls (solid blue line).

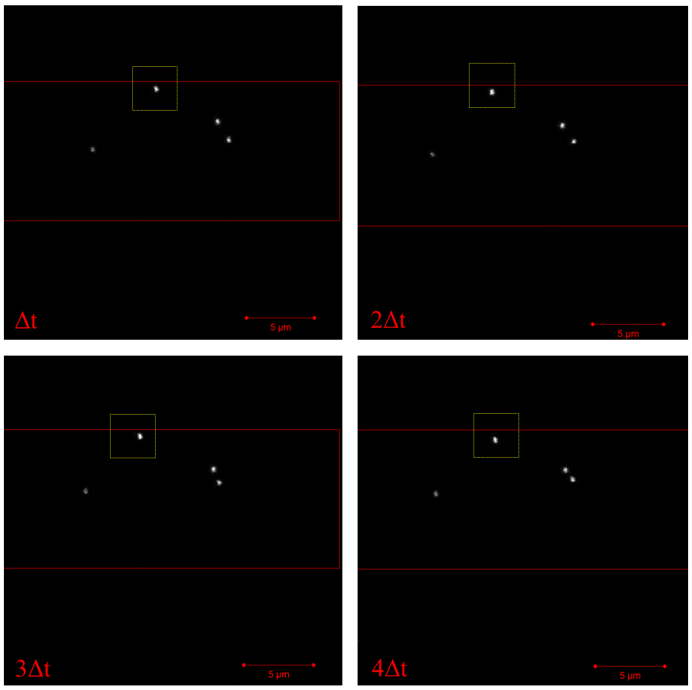


Figure 4.9: Red line marks the boundary of channel side walls in the y-direction. Particle tracked in the images a was the one enclosed inside yellow box. It is an example of a particle travelling very close to the wall. The figure presents four steps taken by the particle after a time interval of Δt.

of $D_{nano}$, a closer look at the videos was taken and the path followed by particles analyzed. Two cases were observed, as presented in Figure 4.8. Few particles followed a path spread throughout the width of the channel (white and green track) while few spent most of their time near the side wall in the y-direction (particle with red track).

Very often $D_{nano}$ had a value above $4\times10^{-13}$ $m^2/s$, exhibited by particles that executed random Brownian motion throughout the width of the channel (in the y-direction). The most frequently witnessed value of $D_{nano}$ was $\sim6\times10^{-13}$ $m^2/s$. This was the case for particles with tracks similar to green and white tracks in Figure 4.8. However, for certain cases, $D_{nano}$ exhibited values six times less than what was very frequently observed. Hence, $D_{nano}$ also assumed values of $\sim1\times10^{-13}$ $m^2/s$. This was

observed when particles traversed a path close to the wall (Figure 4.9, particle with red track in Figure 4.8). It was speculated that not only the confining dimensions had an impact on the diffusion coefficient of the 100 nm polystyrene beads, but in certain cases the non-confining walls in the y-direction also played a role. If the research questions are revisited, it shall be noted that the aim of the study was to find the impact of confining dimensions on the diffusion coefficient of the particles. Since, few cases also exhibited an influence of the side walls (non-confining) on the mobility of particles, the analysis was split into two parts. The first part of analysis was for particles in nanochannel which travelled throughout the channel (Section 4.3.2). While the second part of analysis (Section) was for particles in the nanochannel for which a minimum of 50% of the particle positions fell within a distance of 1 $\mu$m from the side wall (as marked out in the Figure 4.8).

### 4.3.2. Diffusion coefficient in the nanochannel without the effect of side wall (in the y-direction)

This section summarizes the results for particles which travelled throughout the width of the nanochannel. The experimental result of diffusion coefficient in nanochannel was compared to $D_{unconfined}$ (obtained in Section 4.2.3) and the extent of confinement effect was quantified. Then follows a discussion on what are the possible factors that result in a different behaviour of solute in nanochannels as compared to microchannels. A discussion on whether the research gap can be bridged is also summarized.

Sample used for particle tracking in the nanochannel was 100 nm polystyrene beads suspended in 30/70 wt% glycerol/demineralized water with 1 mM KCl, the preparation of which is described in Section 3.3. 115 particles with a total of 11061 x and y-displacements each were analyzed to yield the diffusion coefficients ($D_{x,nano}$,$D_{y,nano}$). Particles were tracked using the software described in Section 3.4. Once the frame to frame displacements were obtained, a histogram of these displacements were created. Gaussian fit over the obtained frequency distribution was performed to obtain the 1D diffusion coefficients (Section 3.4.2).

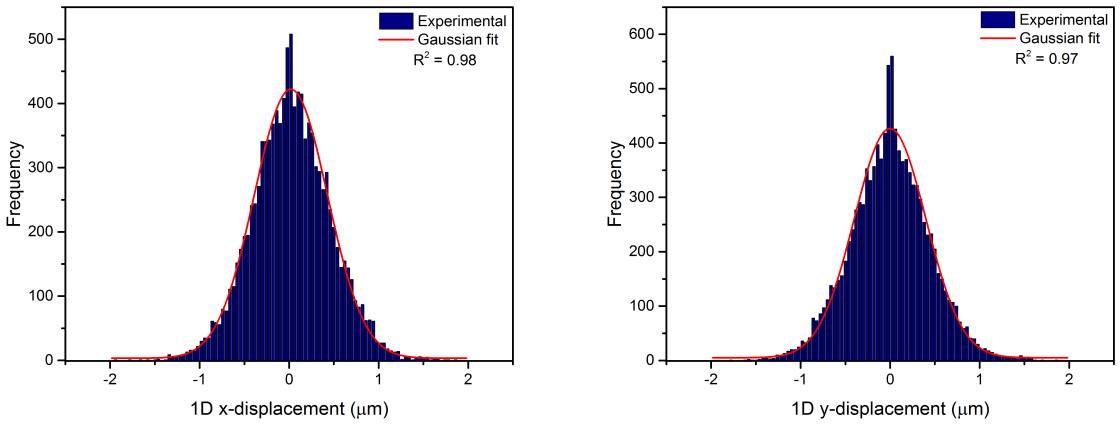


(a) (b)

Figure 4.10: Gaussian fit performed to the frequency distribution of the 11061 (a) x-displacements and (b) y-displacements in the microchannel. The variance from Gaussian fit to x-displacement histogram is 0.1885 $\mu$m$^2$ and the variance from Gaussian fit to y-displacement histogram is 0.1909 $\mu$m$^2$.

Figure 4.10 represents the histogram of 11061 x and y displacements with Gaussian fit performed over it. The mean from the Gaussian fit to the x and y displacement histogram was found to be 27.5 nm and 2.9 nm respectively. For a displacement of 27.5 nm, the contribution by velocity/drift is ~400 times less than that by diffusion[70]. It will be clearly much smaller for a displacement of 2.9 nm. Hence, it can be concluded that convection was absent from the experiments. Equation 4.8 was used to

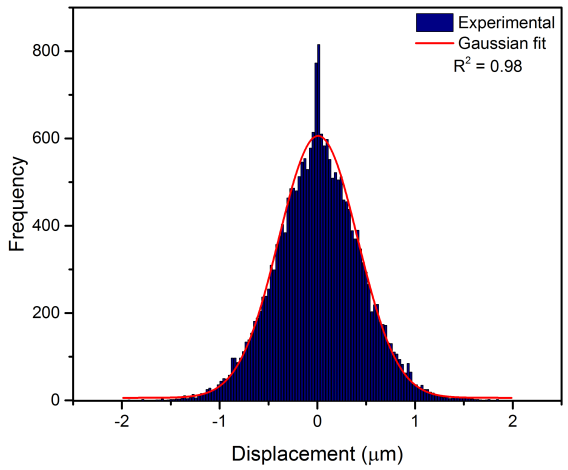


Figure 4.11: Gaussian fit performed to the combined x-displacements and y-displacements in the nanochannel. The variance from Gaussian fit to total displacement histogram is 0.1899 $\mu m^2$.

Table 4.4: Summary of the experimental results of diffusion coefficients as obtained in the nanochannel.

| Diffusion coefficients ($m^2/s$) | | |
|---|---|---|
| $D_{x,nano} \times 10^{13}$ | $D_{y,nano} \times 10^{13}$ | $D_{nano} \times 10^{13}$ |
| $6.78 \pm 0.09$ | $6.86 \pm 0.09$ | $6.83 \pm 0.06$ |

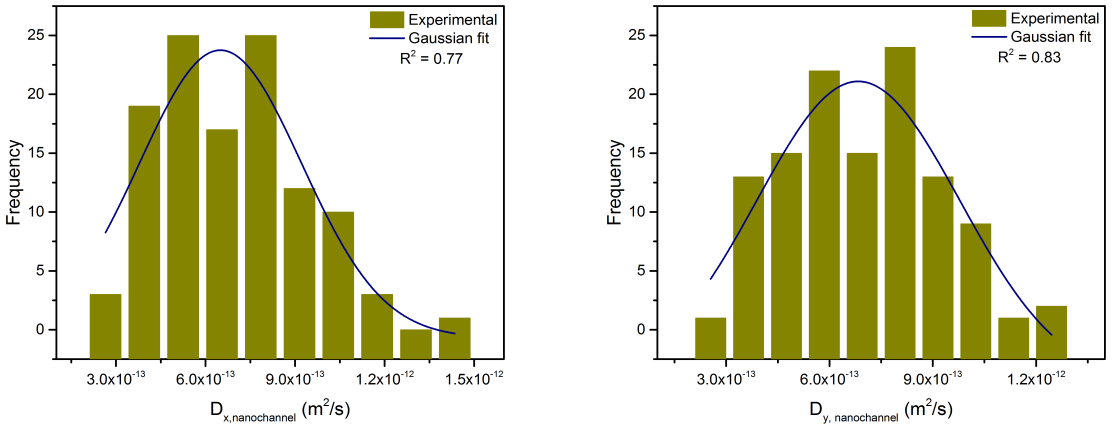


(a) (b)

Figure 4.12: Distribution of (a) $D_{x,nano}$ and (b) $D_{y,nano}$ of individual 100 nm polystyrene beads in nanochannel of height 300 nm, varying width ( 5 and 10 $\mu$m) and varying length (15-200 $\mu$m)

estimate $D_{x,nano}$ and $D_{y,nano}$ where, $\langle \Delta x^2 \rangle$ and $\langle \Delta y^2 \rangle$ is equivalent to the variance of the fit performed and $\Delta t$, the time between displacements, is 0.139 s (Section 3.3). To obtain the average diffusion coefficient ($D_{nano}$), a histogram of both the x and y displacement was created, Gaussian fitting was performed over the distribution (Figure 4.11) and the variance from the fit was used. The values of diffusion coefficient obtained from the experiments are presented in Table 4.4.

The uncertainty of $\pm 0.09$ and $\pm 0.06$ in the experimental results is the sampling error, which depends

on the number of data points in the histogram [63] and was estimated in the same way as it was for particle tracking in microchannel(Section 4.2.2). Figure 4.12 further shows the distribution of diffusion coefficients of the individual particles inside the nanochannel. The most frequent $D_{x,nano}$ was $6.56\times10^{-13}$ m$^2$/s with a standard deviation of $2.62\times10^{-13}$ m$^2$/s while the most frequent $D_{y,nano}$ was $6.78\times10^{-13}$ m$^2$/s with a standard deviation of $2.74\times10^{-13}$ m$^2$/s. The diffusion coefficients fell into a broad range and this spread can be attributed to the effect of confinement, which will be discussed in the following sections. The distribution of diffusion coefficients of individual particles is interesting to see as it throws light on the existing heterogeneity within the same system. It can be imagined that how inside an actual biological cell, each solute or particle might be experiencing different degree of confinement at a given instant of time.

### Comparison of diffusion coefficient in nanochannel ($D_{nano}$) with unconfined diffusion coefficient ($D_{unconfined}$)

Particle tracking in nanochannel revealed that the average diffusion coefficient of 100 nm polystyrene beads in 300 nm high channels was $(6.83 \pm 0.06)\times10^{-13}$ m$^2$/s ($D_{nano}$). However if the same particles were tracked in the same solvent medium of 30/70 wt% glycerol/water mixture in an unconfined bulk system, the diffusion coefficient was $(14.31 \pm 1.04)\times10^{-13}$ m$^2$/s ($D_{unconfined}$), as obtained in Section 4.2.3. A noticeable difference is seen between the two values of diffusion coefficients of $D_{nano}$ and $D_{unconfined}$. It is pertinent to quantify the extent of deviation observed in confined system as compared to bulk systems to draw conclusions about the possible effects of confinement. The ratio of the values of diffusion coefficients is estimated to be:

$$\frac{D_{nano}}{D_{unconfined}} = \frac{(6.83 \pm 0.06) \times 10^{-13}}{(14.31 \pm 1.04) \times 10^{-13}} = 0.48 \pm 0.03 \tag{4.12}$$

In calculating the above resultant ratio of $D_{nano}$ to $D_{unconfined}$, rules of error propagation was followed [64]. Hence, in the confined system under investigation, a reduction in the mobility of 100 nm polystyrene beads of about ~52% was observed. Following section attempts at describing the possible phenomena that result in the retarded mobility of particles in nanochannels.

### Evaluating confinement through different lenses

Experimental investigations of 100 nm particle tracking in 300 nm high nanochannel revealed that there was a significant reduction of mobility of the particles as compared to bulk system. The ratio of $\frac{D_{nano}}{D_{unconfined}}$ was found to be $0.48 \pm 0.03$. Hence, as per the study conducted, the maximum and minimum values of the ratio of confined diffusion coefficient to the unconfined diffusion coefficient were 0.45 and 0.51 respectively. In order to explain the deviation of observed diffusion coefficient from $D_{unconfined}$, multiple effects (hydrodynamic interactions, electrical double layer, Van der Waals forces and solvent viscosity) have been considered and are as discussed below.

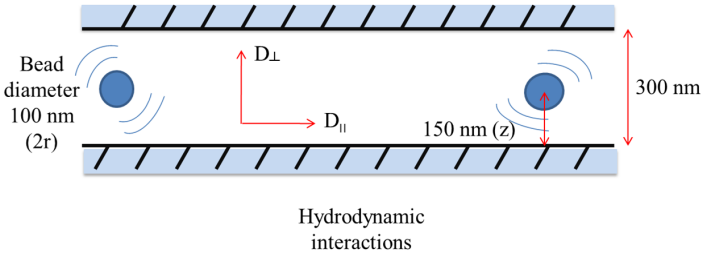


Figure 4.13: Schematic representation of 100 nm particle diffusing in nanochannels 300 nm high. Hydrodynamic interactions between particle and wall affect the parallel(x and y direction), $D_{\parallel}$ and perpendicular(z-direction) component, $D_{\perp}$ of diffusion coefficients.

The first factor considered is hydrodynamic interactions with the wall. As explained in Section 2.2.1, when a particle moves, it creates disturbance in the fluid around it that travel through the fluid. In the case, when there is present an obstruction (a wall or another particle) at a finite distance from the

wall, these disturbances damp the motion of particle (Figure 4.13). In the current study, the particle movement was observed in the xy plane while the confinement was in the z direction. The particle size (100 nm) was comparable to the depth of the channel (300 nm) in the z-direction. The presence of the wall at a finite distance from the particle in the z-direction is expected to slow down its movement. The number of particles in the field of view in the experiments were very often 1 or 2. Sometimes a maximum of 3 particles were also obtained within the frame. A minimum inter-particle distance of 2 $\mu$m (20 particle diameter) was seen. Hence particle-particle hydrodynamic interactions are not expected to play a role[32]. The particle wall interactions are expected to have an impact on the mobility of the particle. The particle movement tracked using confocal microscope was a 2D projection of 3D movement. The motion observed was in the xy plane and parallel to the channel walls. Numerical predictions are available that approximate the expected ratio of parallel and perpendicular component of diffusion coefficients to bulk value of diffusion coefficients and give an insight into the deviation from Stokes-Einstein relation. Using these approximations (Equations 2.22 and 2.23), Figure 4.14 summarizes the effect on diffusion coefficient of 100 nm polystyrene beads as a function of the distance from the walls of the nanochannel that are 300 nm high. It can be seen that the movement of the particles perpendicular to the wall is damped much more as compared to the parallel movement. For a particle that is in the centre of the channel (z=150nm), $\frac{D_{\parallel}}{D_{unconfined}}$ and $\frac{D_{\perp}}{D_{unconfined}}$ are expected to be 0.81 and 0.64 respectively. Hence, for the 100 nm polystyrene beads present in the centre of the channel, while the parallel component of diffusion coefficient deviates by around 20% from diffusion coefficients in bulk system, the perpendicular component of diffusion coefficient deviates by nearly 37%. Hence, in the system under investigation, hydrodynamic interactions are always in action. The observed ratio of the parallel and perpendicular component of diffusion coefficient span a whole range. This explains the wide distribution of diffusion coefficients of individual particles in the nanochannel (Figure 4.12).

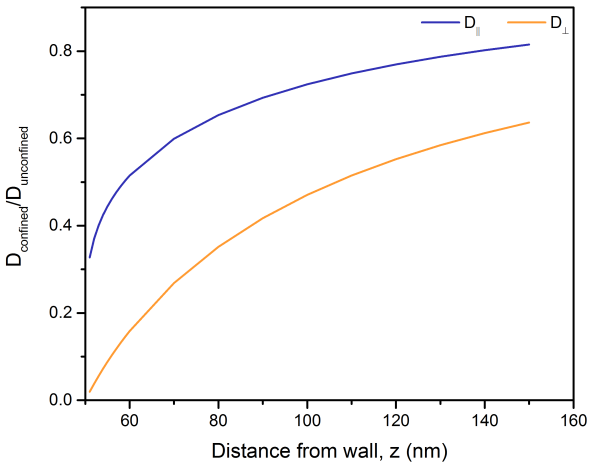


Figure 4.14: Ratio of parallel and perpendicular component of diffusion coefficient in the presence of wall with respect to unconfined diffusion coefficients as obtained from theoretical approximations. [29, 31]. The distance from the wall is the distance of the centre of the particle from the wall as depicted in Figure 4.13.

To further understand the experimentally obtained ratio of $\frac{D_{nano}}{unconfined}$, the study by Faucheux and Libchaber (1994) was explored [76]. They performed numerical and experimental investigations of diffusion of micro-sized silica and latex spheres in water confined between two walls. They observed the x and y coordinates of the moving particle and hence, were followed a 2D projection of 3D movement of the particle. A numerical model was presented in their study by using the numerical approximation and exact solution of the parallel and perpendicular component of diffusion coefficient (Equation 2.20 and 2.21). It was proposed the the motion of the particle observed is the horizontal excursion of the particle in time. However, while following a path in the horizontal xy plane, the particle also moves a distance in the z-direction (perpendicular to the wall). The measured horizontal displacement is averaged over

a vertical distance, the particle is estimated to travel in the same time. This results in the actual averaged diffusion coefficient that would be observed as a result of hydrodynamic interactions of a particle with the walls. In our study, the ratio of the channel height (300 nm) to particle diameter (100 nm) is 3. Faucheux and Libchaber performed experiments for varying ratios of channel height to particle diameter. In one set of experiments they tracked polystyrene beads in water and the channel height to particle diameter ratio was 3. The ratio of confined to unconfined diffusion coefficient was reported to be 0.45 and 0.48, estimated experimentally and numerically respectively [76]. In our experimental investigation the ratio of $\frac{D_{nano}}{unconfined}$ is estimated to be 0.48 $\pm$ 0.03. Hence, the experimental result show agreement with the experimental and analytical results of the study conducted by Faucheux and Libchaber. The agreement substantiates the fact the indeed hydrodynamic interactions play a major role in affecting the mobility of particles in confined systems. Figure 4.14 presents the expected deviation in diffusion coefficient at each height of the particle inside the channel, which is true for the moment the particle attains that particular height. It shall be kept in mind that the resultant observed diffusion coefficient is an average of the effect of movement in the perpendicular and parallel directions. In the study by Hoang et.al. (2011), the mobility of 25 nm quantum dots were studied in nanochannels that were 150 nm high[37]. The observed ratio of $\frac{D_{confined}}{D_{bulk}}$ in their experimental investigation was found to be ~0.35. It has been reported that due to hydrodynamic interactions the ratio of mobility in confined system to a bulk system would be only 0.88. They concluded that hydrodynamic interactions cannot explain the extent of deviation observed in their experiments. The value of 0.88 was reported by using Equation 2.21 and under the assumption that the particle stays in the centre of the channel at a height of 65 nm. However, the particle is not expected to stay in the centre of channel at all times. It will traverse the entire height of channel approaching much closer to the wall. Moreover, while the x and y coordinates were tracked, it is important to not lose sight of the fact that the particle also moves in the z-direction at the same time. It is speculated that the model of Faucheux and Libchaber could provide a more correct estimate of the contribution of hydrodynamic interactions in retarding the mobility of quantum dots for their study.

The second lens through which the experimental results should be analyzed is the interaction of the particle with electrical double layer and Van der Waals forces. The experiments were performed using 100 nm polystyrene beads suspended in a solvent medium of 30/70 wt% glycerol/demineralized water mixture with KCl salt concentration of 1 mM. These polystyrene beads are coated with hydrophilic polymer and have carboxylic terminal functional groups[54]. Initial experiments proved difficult because the the particles were sticking to the channel walls. In the experiments, the use of salt prevented the sticking of particles to a large extent, though not completely. The purpose behind addition of salt was to prevent adsorption of the particles to the channel walls. The idea is based on competitive interaction between electrical double layer and Van der Waals interaction [77]. The potential energy curves separating two surfaces comprises of two parts: a negative one due to Van der Waals attractive forces and a positive one owing to double layer repulsion. This forms a resultant curve. Under favorable conditions the repulsion between surfaces due to double layer is sufficient enough to keep the surfaces from sticking from each other. This offers a probable explanation to the observed effect of reduced propensity of particle sticking due to the presence of salt in the experiments. In an investigation by Assemi et. al.(2006), adhesion of carboxylate modified polystyrene spheres suspended in water (with varying concentration of NaCl) to glass surfaces was studied by means of Atomic Force Microscope [78]. It was found that for separation less than ~5 nm, Van der Waals forces dominated and caused the particle to stick to the glass surface. Based on the aforementioned findings, choice of using 1 mM salt was made. The presence of 1 mM KCl salt in the aqueous solvent and charged surfaces in the system under investigation is expected to result in a double layer of thickness ~9 nm (calculated using Equation 2.24). Furthermore, the role played by Van der Waals forces is evaluated. As these forces are significant only within a range of few nm (less than 5 nm), it is likely that Van der Waals force do not play a significant role in damping the particle's motion in the system under consideration.

Moving on, the interactions with the electrical double layer can be expected to have an impact on the diffusion behaviour of 100 nm latex beads in 300 nm high nanochannels. However, the discussion and comparison of experimental results with findings from literature in the preceding paragraphs, suggest that hydrodynamic interaction is infact the main contributing factor in reducing the mobility

of the particles in the nanochannel. What role could the double layer be playing? The thickness of double layer in the experiments is much smaller than the particle and channel size and double layer overlap is not expected. In the work done by Feitosa and Mesquita(1991), it has been reported that there exists an equilibrium position for particles resulting from the total potential energy profile due to double layer and gravitational field[35]. The probability of finding a particle at distances smaller than the equilibrium position decays abruptly (Section 2.2.2). Hence, the number density closer to the walls is expected to be less. The equilibrium position acts a mirror and reflects the particle, not allowing it to approach closer to the wall. Moreover, the particles and walls in the system under investigation are both negatively charged. This is the case similar to investigated by Durand et. al. (2009). Hence, it might also be the case that the thickness of the double layer is sufficient to keep the charged particles from interacting with the walls, as discussed in Section 2.2.2 [34]. This could be a probable explanation of the role played by the double layer present in the system.

Electroviscous drag is also evaluated. It should be noted that the 100 nm polystyrene beads used in the experiments were negatively charged due the presence of carboxylic terminal functionality. Even though double layer overlap did not exist in the system, the thin double layer around the particle could slow down the mobility of the particle. When a particle moves due to thermal agitation, the ions in the diffuse layer of the electrical double layer are dragged along with its motion. This is the electroviscous effect that is known to retard the motion of solute [37]. In the system under investigation the thin double layer (~9 nm) around polystyrene beads (r = 50 nm) is not expected to slow down its mobility. This conclusion is drawn on the basis of investigations by Schumacher et. al.(1987), where effect on Brownian motion due to drag force by double layer around colloidal particles was studied[79]. They found that for $\kappa r \approx 5$ (the condition relevant to this study), where $\kappa^{-1}$ is Debye length and r is the particle radius, the diffusion coefficients of negatively charged latex beads surrounded by an ion cloud of $Na^+$ and $Cl^{-1}$ were not affected. It was only for $\kappa r$ less than 2 that the diffusion coefficients of particles were affected by electroviscous drag. It should also be noted that the extent of reduction of diffusion coefficients due to the presence of double layer around the particle also depends on the type of ions surrounding the particle.

However, in some cases, there are chances of overlap of electrical double layer and electroviscous effects might severely damp the mobility of the particle, unlike the situation in our experiments. In the investigation by Eichmann et. al.(2007), trajectories of 50-250 nm charged gold particles was studied in channels that were 300-600 nm high. Debye length was maintained thick enough ($(\kappa r) \approx 1$-3), to cause an overlap of the double layer at all times in the channel (Figure 4.15). They reported an experimental result that was still ~50% off from the predictions by hydrodynamic theory. They speculate that the reason behind this discrepancy could be electroviscous drag. Similar arguments are presented by Hoang et. al.(2011) to explain the reduced mobility of 25 nm quantum dots in 150 nm high nanochannels who suspected a double layer comparable to particle size.

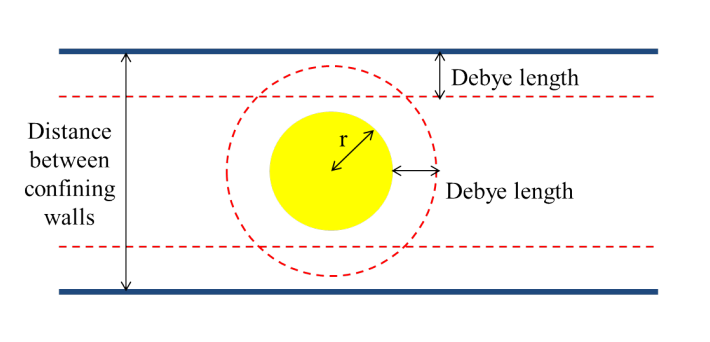


Figure 4.15: Schematic representation of the a system where double layers are thick enough to cause an overlap and contribute to electroviscous drag (r is the particle radius) [36].

Increased viscosity or an apparent change of solvent bulk viscosity is also evaluated as the reason behind reduced mobility. In our experiments, the reduced mobility is predominantly because of

hydrodynamic interactions and agrees well the theoretical predictions. This points at the fact there is no apparent change of solvent bulk viscosity. However, local viscosity increase can be disputed. The solvent used in the experimental study is 30/70 wt.% glycerol/water mixture. The channel walls are PDMS on three sides and glass on one side. A major fraction of solvent is water, which is known to not wet PDMS. As per the investigation by Gao et. al.(2007), with water in contact with glass surface, viscosity increases by about 4 times the bulk viscosity within 2 nm of distance from the wall [40]. While for water next to a non-wetting surface, there did not seem to be any change in local viscosity. If the findings of Gao et. al. are true then increased local water viscosity can be expected near the glass side of channel while there might or might not be a change of viscosity on the PDMS wall side (glycerol-PDMS interaction might have an impact). Kaji et. al.(2006) investigated mobility of 50 nm carboxylate modified polystyrene beads in channels that were 400 nm high [43]. They reported a 3 times reduced diffusion coefficient and attributed it to increased solvent bulk viscosity. However, if only local viscosity increases as per the other investigations, there must be another way to explain their experimental results: hydrodynamic interactions or interactions with double layer. For the 50 nm particle staying in the centre of channel, the ratio of particle size to channel height is 3.5. As per hydrodynamic numerical predictions, the parallel component of diffusion coefficient will be reduced by ~15% and the perpendicular component by ~30% (Figure 2.5). Moreover the particle would travel throughout the channel and would experience further retardation of mobility. There could be also possibilities of electroviscous forces playing a role due to the presence of ions in water.

To conclude, the experimental result of $\frac{D_{nano}}{D_{unconfined}} = 0.48 \pm 0.03$ is found to agree well with predictions by hydrodynamic theory. It is speculated that in the system and length scales under investigation, hydrodynamic interactions play a significant role in affecting the mobility of 100 nm bead. The presence of double layer probably is speculated to only behave as a reflecting mirror favouring a certain distribution of particles inside the nanochannel. Van der Waal forces are present but only within a small range from the wall where the probability of finding a particle is much less and hence, the effect of this does not show on the reduced mobility. Based on the observed results, it may also be concluded that there is no bulk increased viscosity. However, there might be local viscosity variations within a few nm from the wall. It shall also be concluded that investigations carried out in this study cannot fully expel the research gap. Firstly, the system under investigation had a double layer much smaller than the particle size and channel height. Though the observations made in this study seem to agree with findings in literature studying a similar environment, conclusions pertaining to overlapping double layer cannot be made. There exists claims of not sufficient theory to explain the kind of effect overlapping double layers have. It has been reported that in such a case hydrodynamic interactions or electrostatic interactions cannot fully explain the experimentally observed greatly reduced mobility of analytes in confined systems. Moreover, based on the experimental results it is only postulated that there is no bulk solvent viscosity increase (as claimed by few studies) and local viscosity variations near the wall may or may not be present. Hence, it is important to quantify that viscosity variations in the system under investigation. Since, the nature of solvent and surface in contact play a role, it is difficult to predict if there is increased viscosity only localized to a small region from the wall or is not present at all.

### 4.3.3. Diffusion coefficient in the nanochannel with the effect of side wall (in the y-direction)

In the preceding section, analysis and result of diffusion coefficient of particles traversing the entire width of nanochannel was presented and discussed. In this section, is described a special behaviour of particles that was observed in the nanochannel. As mentioned in Section 4.3.1, there were cases when few particles would follow a path close to the side wall. This was interesting to observe as there was no confinement in the y-direction. Yet few particles sometime would happen to travel near the sidewall in the y-direction and produce a different effect. This was observed for about 12% of the total displacements collected in the nanochannel. Diffusion of these particles following a path close to the side all was found to be retarded more severely in comparison to the particles that executed a motion throughout the width of the channel. The diffusion coefficient of particles exhibiting such behaviour has been presented. Then follows a discussion on what results in a different behaviour of solute in nanochannels when it travels close to the side wall.

25 particles with a total of 1557 x displacements and y-displacements each were analyzed to yield the diffusion coefficients ($D_{x,nano}$,$D_{y,nanol}$) under the influence of side wall. The histograms of these displacements were created. Gaussian fit over the obtained frequency distribution was performed to obtain the 1D diffusion coefficients (Section 3.4). Figure 4.16 represents the histogram of 1557 x and y displacements with Gaussian fit performed over it. The mean from the Gaussian fit to the x and y displacement histogram was found to be 1.2 nm and 1.3 nm respectively, which indicates about the absence of any external force causing drift.

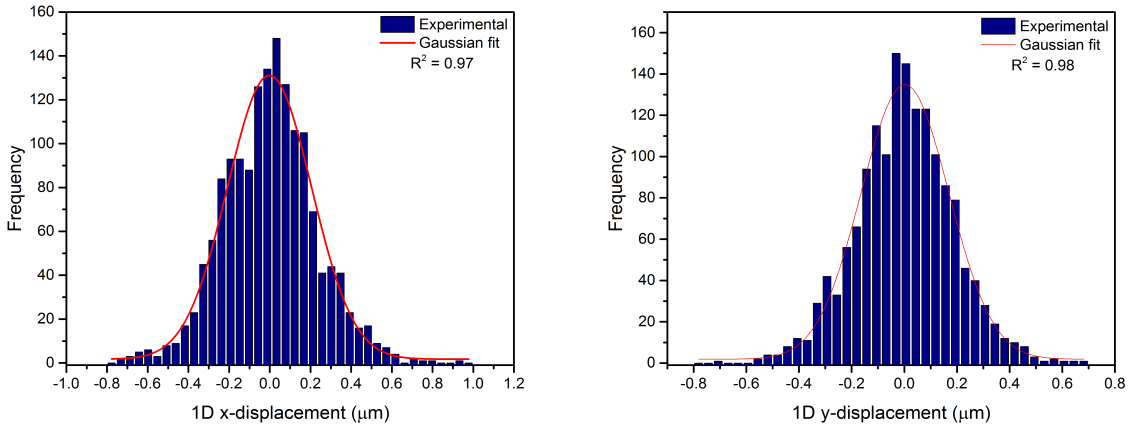


(a) (b)

Figure 4.16: Gaussian fit performed to the frequency distribution of the 1557 (a) x-displacements and (b) y-displacements in the nanochannel. The standard deviation from Gaussian fit to x-displacement histogram is 0.0505 $\mu$m$^2$ and the variance from Gaussian fit to y-displacement histogram is 0.0331 $\mu$m$^2$.

Equation 4.8 was used to estimate $D_{x,nano}$ and $D_{y,nano}$ where, $\langle \Delta x^2 \rangle$ and $\langle \Delta y^2 \rangle$ is equivalent to the variance of the fit performed and $\Delta t$, the time between displacements, is 0.139 s (Section 3.3). $D_{x,nano}$ and $D_{y,nano}$ were found to be $(1.82 \pm 0.06)\times10^{-13}$ m$^2$/s and $(1.18 \pm 0.04)\times10^{-13}$ m$^2$/s respectively. The uncertainty of $\pm$0.06 and $\pm$0.04 in the experimental results is the sampling error, which depends on the number of data points in the histogram [63] and is estimated in the same way as it was for particle tracking in microchannel(Section 4.2.2).

The presence of a wall in the y-direction might affect the diffusion coefficients in the x and y direction due to hydrodynamic interactions with the wall. When the movement of the particle close to the side wall is analyzed, movement of the particle in x-direction is now parallel to the wall while the movement in y-direction is perpendicular to the wall. From Figure 4.14, it is evident that hydrodynamic interactions of a particle moving normal to a wall retards its mobility more severely than for a particle moving parallel to a wall. This is in agreement with experimental results, the nominal value of $D_{x,nano}$ being ~1.5 times $D_{y,nano}$. When $D_{x,nano}$ and $D_{y,nano}$ are compared to each other, they lie 3.5 standard deviations away from each other. Hence, the two diffusion coefficients are anisotropic as result of the presence of the side wall in the y-direction. .

### Evaluating the effect of side wall on diffusion in the nanochannel

In this section, a comparison is drawn between diffusion coefficients to underline the extent of the impact of the presence of sidewall on with particle's movement (Table 4.5).

Particle tracking close to the side wall revealed that the particles would approach as close as ~150 nm from the wall and would remain within 1 $\mu$m of distance from the wall for most time. At separations of the aforementioned magnitude, hydrodynamic interactions are expected to play a role. Hence, results the anisotropy in x and y component of diffusion coefficients, discussed previously. It is seen that the x-component of particle diffusion coefficient under the influence of side wall deviates from the

Table 4.5: Summary of the experimental results of diffusion coefficients.

| Diffusion coefficients × $10^{13}$ ($m^2/s$) | | | |
|---|---|---|---|
| | $D_{nano}$ (side wall influence) | $D_{nano}$(no side wall influence) | $D_{unconfined}$ |
| x-component | 1.82 ± 0.06 | 6.78 ± 0.09 | 14.31 ± 1.04 |
| y-component | 1.18 ± 0.04 | 6.86 ± 0.09 | 14.31 ± 1.04 |

nominal value of $D_{nano}$ in the nanochannel without side wall influence (measured in Section 4.3.2) by ~74%. The y-component on the other hand shows a deviation of ~83%. The effect of three walls present in the vicinity of the particle produce a severe impact on the mobility of the particle causing a reduction of ~90% from mobility in unconfined systems ($D_{unconfined}$). Furthermore, the local diffusion coefficients (in the x-direction,$D_x$) as a function of particle distance from side wall is depicted in Figure 4.18.

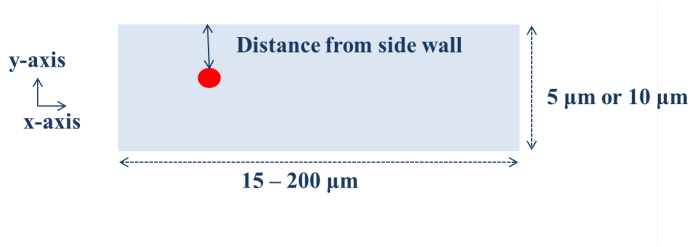


Figure 4.17: Schematic representation of the top view of nanochannel. The distance of the centre of the particle from side wall affects its mobility.

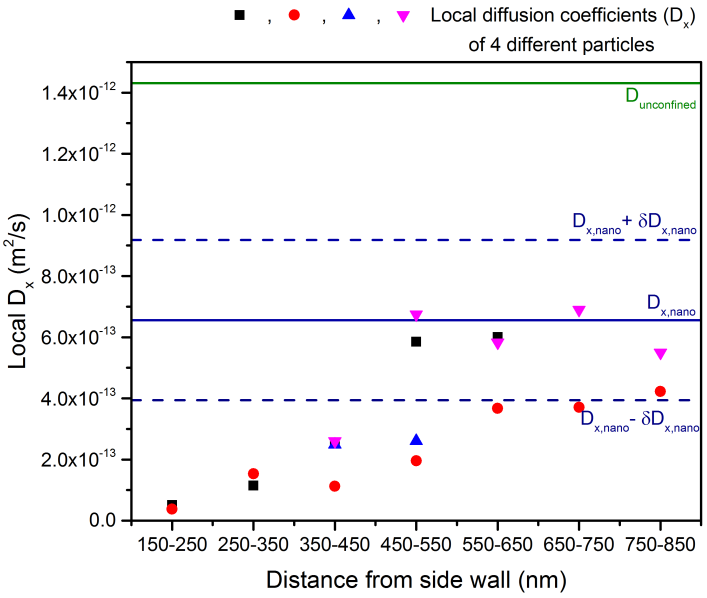


Figure 4.18: Local 1D diffusion coefficients ($D_x$) for 4 different particles as a function of distance from side wall.

To obtain the local diffusion coefficients($D_x$), the y-positions from side wall were rounded off to one significant digit to get enough number of x-displacements corresponding to a particular y-location (hence, the range on the x-axis in Figure 4.18). This generates sufficient number of bins to get reliable estimate of local diffusion coefficient in the x-direction. Figure 4.18 depicts local x-component of diffusion coefficient as a function of distance from side wall for 4 different individual particles. The solid and dashed straight blue lines marked out in the figure correspond to the most frequently occurring

$D_{x,nano}$ ($6.56\times10^{-13}$ $m^2/s$) with a standard deviation of $2.62\times10^{-13}$ $m^2/s$, for individual particles in the nanochannel without the influence of side wall (Figure 4.12).

It becomes evident that after a distance of about 500 nm, that is after 5 particle diameters, the individual particle diffusion coefficients assume values that lie within one standard deviation of the frequently occurring diffusion coefficient. From hydrodynamic predictions for a movement parallel to a wall, for a distance of 5 particle diameters away from the wall, the impact is nearly negligible (Figure 2.5). The effect on the parallel mobility of particles at a distance of 5 particle diameter from the wall amounts to only ~5%. This validates the trend observed for local diffusion coefficients ($D_x$) in Figure 4.18. A similar trend would be expected for the y-component of local diffusion coefficients. For the motion of the particle perpendicular to a wall at a distance of 5 particle diameters from the wall, the impact on mobility drops to ~10%.

To conclude, it shall be noted that an interesting behaviour was displayed by particles in the hybrid micro/nanofluidic device. The nanochannels were designed to have the confining dimension of 300 nm in the z-direction while the length and width (in the x and y direction) were dimensions in microns. It is important to note that despite the absence of confinement in the y-direction, there were instances when particles would travel close to the wall. This resulted in reduced mobility of particles as compared to mobility otherwise observed in the nanochannel. This also made $D_{x,nano}$ and $D_{y,nano}$ anisotropic. It was observed that once a particle by random chance approached a side wall, very often it tended to spend some time near the side wall despite no confinement in the y-direction. It is speculated that this happened because of the confinement in z-direction. Particle location close to a side wall led to a situation where it moved perpendicular to two walls, which leads to severe retardation in mobility. Moreover, such a behaviour gives an insight into what could be expected for future experiments. In the case of use of high concentration of particles, the chance of interaction of particles with the side wall would increase. Also, hydrodynamic interactions between two particles would also play a role. An analogy can be drawn from such an observation to biological systems. Solute particles moving close to cell wall or membranes might undergo such an effect making the diffusion coefficients in different directions anisotropic, despite no confinement.

# 5

# Conclusion

A hybrid micro/nanofluidic device was developed that enabled diffusion coefficient measurements in bulk and confined environment. Brownian motion was observed in the micro/nanochannels using Confocal Laser Scanning Microscope, and diffusion coefficients determined using particle tracking method. The research questions to be answered, mentioned in the beginning of the thesis, are stated again. Below each question is summarized the conclusion drawn from the study.

1. Is the experimental method of determining diffusion coefficient reliable?
    - The image and data analysis methods were reliable and optimized. The particles' location were tracked accurately and a minimum of 50 frames per particle were considered to yield reliable estimates of diffusion coefficient.
2. What is the diffusion coefficient of the analyte found in microchannel / bulk system?
    - 6533 particle displacements were collected in the microchannel to yield experimental estimate of diffusion coefficient in bulk. Experimental results were statistically significant and in agreement with theoretical estimate.
3. What is the diffusion coefficient of the analyte found in nanochannel / confined system? By what magnitude do the confining dimensions of the nanochannel cause the diffusion coefficient of the analyte to deviate from the one found in microchannel?
    - 11061 particle displacements were collected in the nanochannel. In the confined system under investigation, the confining depth of 300 nm caused a reduction in the diffusion coefficient of 100 nm polystyrene beads by about ~52% compared to bulk.
    - Few particles exhibited an interesting behaviour close to the side wall along the width of the channel (not confining). This accounted for 1557 displacements (about 12% of the total displacements collected in nanochannel). The diffusion coefficient of particle near side wall reduced by around ~90% relative to bulk while also making the x and y component of diffusion coefficients anisotropic.
4. What factors are responsible for yielding the diffusion coefficient as obtained in the nanochannel?
    - The experimental results were in agreement with the long standing analytical predictions of hydrodynamic theory. The electrostatic interactions with double layer smaller than particle size did not seem to retard the particles' mobility. Van der Waal forces, strong only within a small range from the wall, are also speculated to not have an impact on mobility. Claims of increased bulk viscosity might be rejected while it might be difficult to make conclusive remarks about local viscosity changes.
    - It was also found that the particles' mobility reduced greatly due to hydrodynamic interactions if it were within a distance of 5 particle diameters from the non-confining sidewall. This also gives an insight into how an analyte would behave in cellular systems - diffusion of analytes close to cell membranes or wall might undergo such an impact.

5. Can the ambiguity be expelled or research gap filled?

   - Investigations carried out in this study cannot fully expel the research gap. Firstly, there exists claims of not sufficient theory to explain the kind of effect overlapping double layers have. It has been reported that in such a case hydrodynamic interactions or electrostatic interactions cannot fully explain the experimentally observed greatly reduced mobility of analytes in confined systems. The system under consideration had a double layer much smaller than the particle size and conclusions about overlapping double layers cannot be made. Moreover, based on the experimental results it is only postulated that there is no bulk solvent viscosity increase (as claimed by few studies) and local viscosity variations near the wall may or may not be present. Hence, few more studies in the above discussed directions are required.

.

# 6

# Recommendation

In order to bridge the research gap further, few more investigations have been proposed which are as listed below:

- Investigations of local viscosity increase for water and glycerol/water mixture at a PDMS and glass surface must be carried out. This is required for validating the investigations by Gao et. al.(2007), that report no viscosity increase for water next to a hydrophobic surface while viscosity increase is observed only upto a few nm from a hydrophilic surface. It is important to quantify the viscosity changes due to solvent change. It would substantiate the conclusions drawn from this study.
- Experimental investigations of enhanced electroviscous effects are known to be scant [36]. Hence, investigating diffusion of an analyte in a confined system wherein the size of double layer is significant and electroviscous effect is dominant is proposed. The experimental conditions must be chosen such that overlapping double layer conditions are observed. The diffusion coefficient resulting from such an analysis would first produce an experimental evidence of the reduction in mobility, if any, deviating greatly from hydrodynamic predictions due to enhanced electroviscous effect. The results then should be compared to similar studies reported in literature and matched with analytical predictions to validate if there is indeed not a suitable theory that can explain/predict the diffusion behaviour of a particle in systems.

The aforementioned recommendations would be able to dismiss the research gap while allowing to move to the next stage of the project. In the next level, diffusion in the confining nanochannels must be investigated in the presence of crowding agents. Crowding with confinement would mimic the actual biological cell environment. It is important to understand how the diffusion behaviour of analyte would further respond to the presence of dynamic changes (due to the crowding agents packed around analyte of interest) in the confining environment, which in turn affect the rate of enzymatic reactions.

# List of Figures

# List of Tables

# A

# Height profile of channels in PDMS

The master (silicon wafer with the pattern of microchannels and nanochannels) created using photolithography was used to perform soft lithography. The pattern of channels on silicon wafer were transferred into PDMS. It was important to characterize the depths of these channels in PDMS to be certain about the size range of the channels. Atomic Force Microscope (AFM) was employed to measure the depth of the nanochannels and microchannels. The depth of the nanochannel was found to be ~300 nm, the same as observed for the channels on master (Figure A.1). However, the height of microchannels in PDMS was found to be ~3 $\mu$m (Figure A.2) while the height of channels measured on the master was ~4.5 $\mu$m. This measurement was an indication towards the inability of measuring depths/heights beyond 3 $\mu$m using AFM.


Figure A.1: Left: 3D profile of nanochannel in PDMS captured using AFM. 0 on the y-axis corresponds to the bottom surface of the nanochannel. Right: Channels in PDMS. Red line indicates the position along which depth measurement was performed.

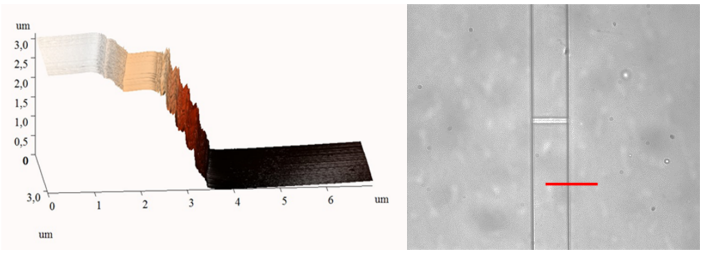


Figure A.2: Left: Depth of microchannel in PDMS as measured using AFM. 0 on the y-axis corresponds to the bottom surface of the microchannel. Right: Channels in PDMS. Red line indicates the position along which depth measurement was performed.

Therefore, the depth of microchannel in PDMS was measured again using profilometer and was found to be ~4.5 $\mu$m (Figure A.3). This was in agreement with the height profile of channels as obtained for the master. Hence, the height of the channels as obtained on the silicon wafer, was transferred reliably into the PDMS stamp.

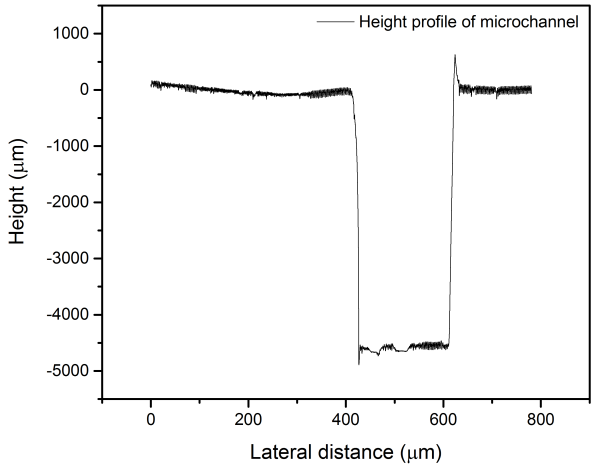


Figure A.3: Depth of microchannel in PDMS obtained as a result of soft lithography. Measurement was done using profilometer. Negative height is an indication of the channels present as valleys in PDMS.

# B

# Height profile of channels on silicon wafer

Channel profiles were obtained at various locations in the master and it was found that the heights of the channels were on an average 4.5 $\mu$m and 300 nm for the microchannel and nanochannel respectively. A sample height profile of the channels was presented in Figure 3.6. Height profile at another location in the master is presented by the following Figures B.1 and B.2.

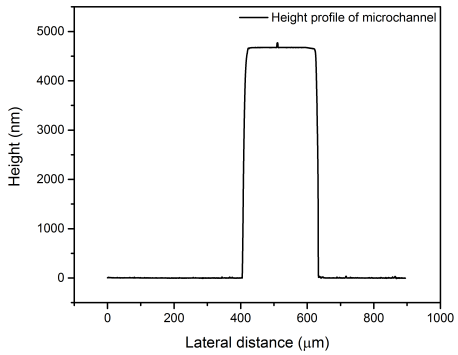


Figure B.1: Height of microchannel as obtained on silicon wafer as a result of photolithography. Height characterization done by profilometer.

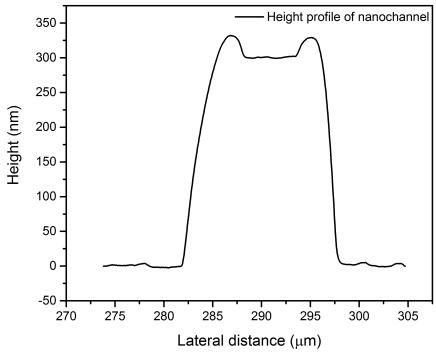


Figure B.2: Height of nanochannel as obtained on silicon wafer as a result of photolithography. Height characterization done by profilometer.

# C

# Hydrophilic treatment of PDMS

Attempts were made to make the surface of PDMS hydrophilic by opting for two different methods: thermal aging and treatment by sodium hydroxide.

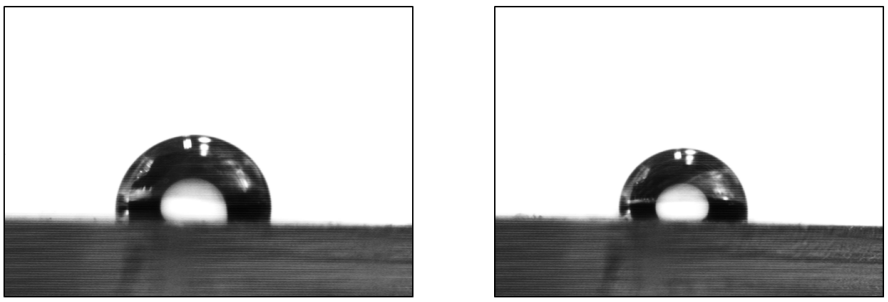

Figure C.1: Water contact angle measured on treated PDMS surface was found to be ~94 degrees. PDMS was cured over a week at 343 K and treated with 1M NaOH for 3 hours.

Thermal aging involves curing the PDMS at higher temperatures for days [81]. It was found in an investigation by Eddington et. al.(2006) that curing PDMS blocks at 373 K for 2, 4, 7 and 14 days damped the process of hydrophobic recovery. Hydrophobic recovery time was found on the basis of contact angle measurements. The best effect was observed for PDMS sample cured for 14 days at 373 K, wherein the PDMS water contact angle remained less than 50 degrees until 10 days. It was suggested by the study that curing at higher temperatures (but less than 473 K) for less number of days, would produce the same effect. On the basis of the results of this study, extended curing was performed at 343 K for 7 days. Contact angle measurements were performed. The PDMS water contact angle remained more than 90 degrees (Figure C.1). Hence, this attempt of extended curing at temperatures less than 373 K did not seem to make the PDMS hydrophilic. It is recommended to follow the same experimental protocol as suggested by Eddington et. al.(2006) in order to verify the results of their study.

A second attempt of making PDMS hydrophilic was to treat PDMS with 1M NaOH [82] for 1 and 3 hours. It was expected that NaOH treatment would lead to an increase in surface -OH groups rendering PDMS hydrophilic. However, contact angle experiments revealed that the surface continued to remain hydrophobic. This was in line with the findings of Hoek et. al.(2010). They reported that NaOH treatment did lead to cleavage of Si-O-Si and Si-$CH_3$ bonds but it did not lead to an increase of silanol (Si-OH) groups. They speculate that NaOH treatment probably results in an increase of C-OH groups on the surface. However, NaOH treatment of PDMS does have benefits when it comes to increasing electrosmotic flow through channels. This might prove helpful in studying biological systems which usually involve working with buffer solutions.

# D

# Working principle of confocal laser scanning microscope

In order to visualize the fluorescent polystyrene beads in the channels, confocal laser scanning microscope is used. In the following paragraphs there is a brief summary of the working principle of confocal microscope and the imaging parameters used.

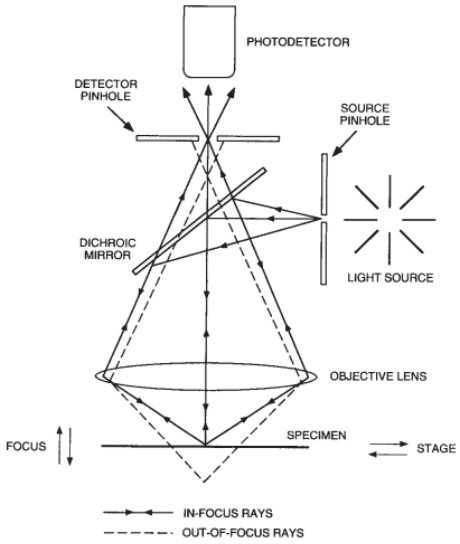


Figure D.1: Light path in a laser scanning confocal microscope [80].

Figure D.1 shows the light path followed in a typical confocal microscope [80]. Imaging using confocal microscope follows the method of scanning focused beam of light across the specimen. The point source of light from a pinhole is focused by the objective lens onto the specimen through a dichroic mirror. The dichroic mirror is a beamsplitter that behaves as a mirror for the excitation wavelength and transparent to all the other wavelengths. The excitation of the specimen leads to the emission of light. The emitted wavelength then passes through the dichoric mirror to the detection pinhole. The arrangement of pinhole is such that it enables to reject the out of focus light and accepts light coming only from a narrow focal plane. This allows to capture high resolution images. The resolution in the xy and z direction are given by [83]:

$$R_{xy} = \frac{0.4\lambda}{NA} \tag{D.1}$$

$$R_z = \frac{1.5\lambda RI}{NA^2} \tag{D.2}$$

where *NA* is numerical aperture of lens, $\lambda$ is detected wavelength and *RI* is refractive index of immersion liquid.

Resolution ensures that two fluorescent objects as viewed by the microscope appear as two distinct objects only when they are sufficiently far enough. Depth of focus on the other hand is an estimate of the axial distance between two blurred images. It is the optical slice thickness which is imaged in good focus. It is referred to as full width at half maximum (FWHM) and is given by:

$$FWHM = 0.86R_z \tag{D.3}$$

Care should always be taken to make sure that pinhole size is not smaller then the depth of focus which deteriorates the quality of images due to loss of light.

# Bibliography


[1] A. S. Verkman, *Solute and macromolecule diffusion in cellular aqueous compartments,* Trends in biochemical sciences **27**, 27 (2002).

[2] L. Bocquet and E. Charlaix, *Nanofluidics, from bulk to interfaces,* Chemical Society Reviews **39**, 1073 (2010).

[3] Y. Kazoe, K. Mawatari, and T. Kitamori, *Behavior of nanoparticles in extended nanospace measured by evanescent wave-based particle velocimetry,* Analytical chemistry **87**, 4087 (2015).

[4] K. Mawatari, T. Tsukahara, and T. Kitamori, *Extended nanospace chemical systems on a chip for new analytical technology,* Analyst **136**, 3051 (2011).

[5] H.-X. Zhou, G. Rivas, and A. P. Minton, *Macromolecular crowding and confinement: biochemical, biophysical, and potential physiological consequences,* Annu. Rev. Biophys. **37**, 375 (2008).

[6] A. P. Minton, *Confinement as a determinant of macromolecular structure and reactivity,* Biophysical Journal **63**, 1090 (1992).

[7] C. Wang, D.-K. Ye, Y.-Y. Wang, T. Lu, and X.-H. Xia, *Insights into the "free state" enzyme reaction kinetics in nanoconfinement,* Lab on a Chip **13**, 1546 (2013).

[8] R. J. Ellis, *Macromolecular crowding: obvious but underappreciated,* Trends in biochemical sciences **26**, 597 (2001).

[9] N. A. Chebotareva, D. O. Filippov, and B. I. Kurganov, *Effect of crowding on several stages of protein aggregation in test systems in the presence of $\alpha$-crystallin,* International journal of biological macromolecules **80**, 358 (2015).

[10] D. Gnutt and S. Ebbinghaus, *The macromolecular crowding effect–from in vitro into the cell,* Biological chemistry **397**, 37 (2016).

[11] A. A. Heikal, *Biomedical optics & medical imaging understanding macromolecular crowding is critical for quantitative cell biology,* .

[12] M. E. Davis, J. D. Madura, J. Sines, B. A. Luty, S. A. Allison, J. Andrew, *et al.*, *[22] diffusion-controlled enzymatic reactions,* Methods in enzymology **202**, 473 (1991).

[13] G.-Q. ZHOU and W.-Z. ZHONG, *Diffusion-controlled reactions of enzymes,* The FEBS Journal **128**, 383 (1982).

[14] S. L. Dettmer, S. Pagliara, K. Misiunas, and U. F. Keyser, *Anisotropic diffusion of spherical particles in closely confining microchannels,* Physical Review E **89**, 062305 (2014).

[15] T. Benesch, S. Yiacoumi, and C. Tsouris, *Brownian motion in confinement,* Physical Review E **68**, 021401 (2003).

[16] F. Martin, R. Walczak, A. Boiarski, M. Cohen, T. West, C. Cosentino, and M. Ferrari, *Tailoring width of microfabricated nanochannels to solute size can be used to control diffusion kinetics,* Journal of Controlled Release **102**, 123 (2005).

[17] W. v. Sparreboom, A. Van Den Berg, and J. Eijkel, *Principles and applications of nanofluidic transport,* Nature nanotechnology **4**, 713 (2009).

[18] P. C. Hiemenz *et al.*, *Principles of colloid and surface chemistry*, Vol. 188 (M. Dekker New York, 1986).

[19] A. Paul, T. Laurila, V. Vuorinen, and S. V. Divinski, *Fick's laws of diffusion,* in *Thermodynamics, Diffusion and the Kirkendall Effect in Solids* (Springer, 2014) pp. 115–139.

[20] E. L. Cussler, *Diffusion: mass transfer in fluid systems* (Cambridge university press, 2009).

[21] H. C. Berg, *Random walks in biology* (Princeton University Press, 1993).

[22] R. F. Mudde, M. T. Kreutzer, and V. V. Steijn, *Molecules and Transport Phenomena* (Delft University of Technology, 2015).

[23] MIT, *Conceptual model for diffusion,* www.co2ntramine.nlhttp://web.mit.edu/1.061/www/diffuse/diffno~1.htm, accessed on 30-05-2017.

[24] J. C. Eijkel and A. Van Den Berg, *Nanofluidics: what is it and what can we expect from it?* Microfluidics and Nanofluidics **1**, 249 (2005).

[25] A. Hibara, T. Saito, H.-B. Kim, M. Tokeshi, T. Ooi, M. Nakao, and T. Kitamori, *Nanochannels on a fused-silica microchip and liquid properties investigation by time-resolved fluorescence measurements,* Analytical Chemistry **74**, 6170 (2002).

[26] W. B. Russel, D. A. Saville, and W. R. Schowalter, *Colloidal dispersions* (Cambridge university press, 1989).

[27] M. Reichert, *Hydrodynamic interactions in colloidal and biological systems*, Ph.D. thesis (2006).

[28] L. Lobry and N. Ostrowsky, *Diffusion of brownian particles trapped between two walls: Theory and dynamic-light-scattering measurements,* Physical Review B **53**, 12050 (1996).

[29] B. Lin, J. Yu, and S. A. Rice, *Direct measurements of constrained brownian motion of an isolated sphere between two walls,* Physical Review E **62**, 3909 (2000).

[30] H. Brenner, *The slow motion of a sphere through a viscous fluid towards a plane surface,* Chemical engineering science **16**, 242 (1961).

[31] X. Bian, C. Kim, and G. E. Karniadakis, *111 years of brownian motion,* Soft Matter **12**, 6331 (2016).

[32] M. D. Carbajal-Tinoco, R. Lopez-Fernandez, and J. L. Arauz-Lara, *Asymmetry in colloidal diffusion near a rigid wall,* Physical review letters **99**, 138303 (2007).

[33] H. Daiguji, *Ion transport in nanofluidic channels,* Chemical Society Reviews **39**, 901 (2010).

[34] N. F. Durand, C. Dellagiacoma, R. Goetschmann, A. Bertsch, I. Märki, T. Lasser, and P. Renaud, *Direct observation of transitions between surface-dominated and bulk diffusion regimes in nanochannels,* Analytical chemistry **81**, 5407 (2009).

[35] M. Feitosa and O. Mesquita, *Wall-drag effect on diffusion of colloidal particles near surfaces: a photon correlation study,* Physical Review A **44**, 6677 (1991).

[36] S. L. Eichmann, S. G. Anekal, and M. A. Bevan, *Electrostatically confined nanoparticle interactions and dynamics,* Langmuir **24**, 714 (2008).

[37] H. Hoang, I. Segers-Nolten, N. Tas, J. van Honschoten, V. Subramaniam, and M. Elwenspoek, *Analysis of single quantum-dot mobility inside 1d nanochannel devices,* Nanotechnology **22**, 275201 (2011).

[38] P. Ghosh, *Dlvo theory and non-dlvo forces,* Nptel. ac. in , 1 (2012).

[39] T. Q. Vo and B. Kim, *Transport phenomena of water in molecular fluidic channels,* Scientific Reports **6** (2016).

[40] J. Gao, R. Szoszkiewicz, U. Landman, E. Riedo, *et al.*, *Structured and viscous water in subnanometer gaps,* Physical Review B **75**, 115415 (2007).

[41] V. Y. Rudyak, A. A. Belkin, D. A. Ivanov, V. A. Andrushenko, *et al.*, *Self-diffusion and viscosity coefficient of fluids in nanochannels,* (2011).

[42] K. Pappaert, J. Biesemans, D. Clicq, S. Vankrunkelsven, and G. Desmet, *Measurements of diffusion coefficients in 1-d micro-and nanochannels using shear-driven flows,* Lab on a Chip **5**, 1104 (2005).

[43] N. Kaji, R. Ogawa, A. Oki, Y. Horiike, M. Tokeshi, and Y. Baba, *Study of water properties in nanospace,* Analytical and bioanalytical chemistry **386**, 759 (2006).

[44] L. Li, Y. Kazoe, K. Mawatari, Y. Sugii, and T. Kitamori, *Viscosity and wetting property of water confined in extended nanospace simultaneously measured from highly-pressurized meniscus motion,* The journal of physical chemistry letters **3**, 2447 (2012).

[45] N. Tas, J. Haneveld, H. Jansen, M. Elwenspoek, and A. Van Den Berg, *Capillary filling speed of water in nanochannels,* Applied Physics Letters **85**, 3274 (2004).

[46] R. Robbins, *Photomask making,* https://www.utdallas.edu/~rar011300/LithographyProcess/PhotomaskMaking.pdf (2007), accessed on 20-06-2017.

[47] D. Mask, *Definitions used,* http://www.deltamask.nl/frames.html, accessed on 20-06-2017.

[48] R. Martinez-Duarte and M. J. Madou, *Su-8 photolithography and its impact on microfluidics,* (2011).

[49] M. Chem, *Su-8 2000 permanent epoxy negative photoresist,* http://www.microchem.com/pdf/SU-82000DataSheet2000_5thru2015Ver4.pdf, accessed on 20-06-2017.

[50] J. C. McDonald and G. M. Whitesides, *Poly (dimethylsiloxane) as a material for fabricating microfluidic devices,* Accounts of chemical research **35**, 491 (2002).

[51] G. C. Lisensky, D. J. Campbell, K. J. Beckman, C. E. Calderon, P. W. Doolan, R. M. Ottosen, and A. B. Ellis, *Replication and compression of surface structures with polydimethylsiloxane elastomer,* J. Chem. Educ **76**, 537 (1999).

[52] D. T. Eddington, W. C. Crone, and D. J. Beebe, *Development of process protocols to fine tune polydimethylsiloxane material properties,* in *7th International Conference on Miniaturized Chemical and Biochemical Analysis Systems* (2003) pp. 1089–1092.

[53] A. Mata, A. J. Fleischman, and S. Roy, *Characterization of polydimethylsiloxane (pdms) properties for biomedical micro/nanosystems,* Biomedical microdevices **7**, 281 (2005).

[54] Thermofisher, *Fluospheres ® fluorescent microspheres,* https://tools.thermofisher.com/content/sfs/manuals/mp05000.pdf (2005), accessed on 14-06-2017.

[55] H. Bruus, *Governing equations in microfluidics,* , 17 (2014).

[56] Olympus, *Basics of inverted microscope,* http://www.olympusamerica.com/files/seg_bio/basics_of_inv-microscope.pdf, accessed on 21-06-2017.

[57] J. C. Crocker and D. G. Grier, *Methods of digital video microscopy for colloidal studies,* Journal of colloid and interface science **179**, 298 (1996).

[58] E. M. Furst, *Particle tracking with matlab,* http://lem.che.udel.edu/sandbox/groups/furstgroupwiki/wiki/7672a/attachments/cf8b1/Handout_particle_tracking.pdf?sessionID=82ac3413901a0939289b4eccd678bc74b2701596 (2015), accessed on 21-06-2017.

[59] A. Radenovic, *Brownian motion and single particle tracking,* Advanced Bioengineering methods laboratory, Ecole polyteachenique federal de Lausanne (2014).

[60] S. L. da Silva, J. T. G. Junior, R. L. da Silva, E. Viana, F. F. Leal, *et al.*, *An alternative for teaching and learning the simple diffusion process using algodoo animations,* arXiv preprint arXiv:1412.6666 (2014).

[61] M. A. Catipovic, P. M. Tyler, J. G. Trapani, and A. R. Carter, *Improving the quantification of brownian motion,* American Journal of Physics **81**, 485 (2013).

[62] I. F. Cornell University, Biotechnology Resource Center, *Zeiss 710 confocal microscope user guide,* http://www.biotech.cornell.edu/sites/default/files/uploads/ImagingDocs/Zeiss, accessed on 12-06-2017.

[63] S. Ahn and J. A. Fessler, *Standard errors of mean, variance, and standard deviation estimators,* EECS Department, The University of Michigan , 1 (2003).

[64] J. Taylor, *Introduction to error analysis, the study of uncertainties in physical measurements* (1997).

[65] R. Dijkema, *Towards rapid extracellular vesicle quantification through nanoparticle tracking in a microfluidic device,* , 28 (2016).

[66] N.-S. Cheng, *Formula for the viscosity of a glycerol- water mixture,* Industrial & engineering chemistry research **47**, 3285 (2008).

[67] J. B. Segur and H. E. Oberstar, *Viscosity of glycerol and its aqueous solutions,* Industrial & Engineering Chemistry **43**, 2117 (1951).

[68] P. Shankar and M. Kumar, *Experimental determination of the kinematic viscosity of glycerol-water mixtures,* in *Proceedings of the Royal Society of London A: Mathematical, Physical and Engineering Sciences*, Vol. 444 (The Royal Society, 1994) pp. 573–581.

[69] F. Chenlo, R. Moreira, G. Pereira, and B. Bello, *Kinematic viscosity and water activity of aqueous solutions of glycerol and sodium chloride,* European food research and technology **219**, 403 (2004).

[70] H. Qian, M. P. Sheetz, and E. L. Elson, *Single particle tracking. analysis of diffusion and flow in two-dimensional systems,* Biophysical journal **60**, 910 (1991).

[71] C. S. C. Unit, *Overlapping confidence intervals and statistical significance,* https://www.cscu.cornell.edu/news/statnews/stnews73.pdf (October 2008), accessed on 14-06-2017.

[72] L. Lyons, *A practical guide to data analysis for physical science students* (Cambridge University Press, 1991).

[73] J. R. Anderson, D. T. Chiu, H. Wu, O. Schueller, and G. M. Whitesides, *Fabrication of microfluidic systems in poly (dimethylsiloxane),* Electrophoresis **21**, 27 (2000).

[74] A. Hammadi, *Electrical conductance, density, and viscosity in mixtures of alkali-metal halides and glycerol,* International journal of thermophysics **25**, 89 (2004).

[75] Z. Hai-Lang and H. Shi-Jun, *Viscosity and density of water+ sodium chloride+ potassium chloride solutions at 298.15 k,* Journal of Chemical and Engineering Data **41**, 516 (1996).

[76] L. P. Faucheux and A. J. Libchaber, *Confined brownian motion,* Physical Review E **49**, 5158 (1994).

[77] E. Verwey and J. T. G. Overbeek, *Theory of the stability of hydrophobic colloids elsevier,* New York, NY (1948).

[78] S. Assemi, J. Nalaskowski, and W. P. Johnson, *Direct force measurements between carboxylate-modified latex microspheres and glass using atomic force microscopy,* Colloids and Surfaces A: Physicochemical and Engineering Aspects **286**, 70 (2006).

[79] G. A. Schumacher and T. G. van de Ven, *Brownian motion of charged colloidal particles surrounded by electric double layers,* Faraday Discussions of the Chemical Society **83**, 75 (1987).

[80] S. W. Paddock, *Principles and practices of laser scanning confocal microscopy,* Molecular biotechnology **16**, 127 (2000).

[81] D. T. Eddington, J. P. Puccinelli, and D. J. Beebe, *Thermal aging and reduced hydrophobic recovery of polydimethylsiloxane,* Sensors and Actuators B: Chemical **114**, 170 (2006).

[82] I. Hoek, F. Tho, and W. M. Arnold, *Sodium hydroxide treatment of pdms based microfluidic devices,* Lab on a Chip **10**, 2283 (2010).

[83] R. H. Webb, *Confocal optical microscopy,* Reports on Progress in Physics **59**, 427 (1996).